

Kernel-estimated Nonparametric Overlap-Based Syncytial Clustering

Israel Almodóvar-Rivera and Ranjan Maitra

Abstract

Standard clustering algorithms usually find regular-structured clusters such as ellipsoidally- or spherically-dispersed groups, but are more challenged with groups lacking formal structure or definition. Syncytial clustering is the name that we introduce for methods that merge groups obtained from standard clustering algorithms in order to reveal complex group structure in the data. Here, we develop a distribution-free fully-automated syncytial clustering algorithm that can be used with k -means and other algorithms. Our approach computes the cumulative distribution function of the normed residuals from an appropriately fit k -groups model and calculates the nonparametric overlap between each pair of groups. Groups with high pairwise overlaps are merged as long as the generalized overlap decreases. Our methodology is always a top performer in identifying groups with regular and irregular structures in several datasets. The approach is also used to identify the distinct kinds of gamma ray bursts in the Burst and Transient Source Experiment 4Br catalog and also the distinct kinds of activation in a functional Magnetic Resonance Imaging study.

Index Terms

kernel density estimation, bandwidth, DEMP, k -means algorithm, GSL-NN, overlap.

I. INTRODUCTION

Cluster analysis [1]–[9] is an unsupervised learning method that partitions datasets into distinct groups of homogeneous observations each. Finding such structure in the absence of group information can be challenging but is important in many applications, such as taxonomical classification [10], market segmentation [11], software management [12]. As such, a number of methods, ranging from the heuristic [4], [5], [13]–[16] to the more formal, model-based [6], [17]–[19] approaches have been proposed and implemented.

Most common clustering algorithms, whether model-agnostic such as k -means [16], [20], [21], or model-based such as Gaussian mixture models [6], [19] yield clusters with regular dispersions or structure. Such algorithms are unable to find groups that are general-shaped or structured, so several additional approaches have been suggested to identify irregularly-shaped groups [22]–[28]. Kernel k -means clustering [22] enhances the k -means algorithm by using a kernel function $\phi(\cdot)$ that nonlinearly maps the original (input) space to a higher-dimensional feature space where it may be possible to linearly separate clusters that were not linearly separable in the original space. Spectral clustering [24] uses k -means on the first few eigenvectors of a Laplacian of the similarity matrix of the data. Both methods need the number of clusters to be provided: in the case of spectral clustering, [24] suggests estimating this number as the one with the highest gap between successive eigenvalues.

Evidence accumulation clustering or EAC [23] combines results from multiple runs of the k -means algorithm with the underlying rationale that each partitioning provides independent evidence of structure that is then extricated by cross-tabulating the frequencies of times (out of the multiple partitionings)

I. Almodóvar-Rivera is with the Department of Biostatistics and Epidemiology at the University of Puerto Rico, Medical Science Campus, San Juan, Puerto Rico, USA.

R.Maitra is with the Department of Statistics, Iowa State University, Ames, Iowa, USA.

This research was supported in part by the National Institute of Biomedical Imaging and Bioengineering (NIBIB) of the National Institutes of Health (NIH) under its Award No. R21EB016212. I. Almodóvar-Rivera also acknowledges receipt of a fellowship from Iowa State University's Alliance for Graduate Education and the Professoriate (AGEP) program for underrepresented graduate students in STEM fields. The content of this paper however is solely the responsibility of the authors and does not represent the official views of either the NIBIB or the NIH.

that each observation pair is in the same group. This frequency table serves as a similarity matrix for hierarchical clustering: implementation can be computationally demanding in terms of CPU speed and memory. On the other hand, [29] developed a nonparametric clustering approach under the premise that each group corresponds to a mode of the estimated multivariate density of the observations. The high-density modes are located and hierarchically clustered with dissimilarity between two modes calculated in terms of the lowest density or number of common points in each mode’s domain of attraction.

More recent work [25]–[28] proposed merging groups found using k -means or model-based clustering (MBC). Such methods fall into the category of what we introduce in this paper as syncytial clustering algorithms, because they yield a cluster structure resembling a *syncytium*, a term that in cell biology refers to a multi-nucleated mass of cytoplasm inseparable into individual cells and that can arise from multiple fusions of uninuclear cells. Syncytial algorithms are similar in that they merge or fuse clusters that originally corresponded to a mixture model component or k -means or regular-structured group. Resulting partitions have groups with potentially multiple well-defined and structured sub-groups. We outline some such algorithms next.

MBC is premised on the idea of a one-to-one correspondence between a mixture component of given density form and group. Such injective mapping assumptions are not always tenable so some authors [25]–[27] model each group as a mixture of (one or more) components. Operationally, we have a syncytial clustering framework where identified mixture components that are not very distinct from each other are merged [25]–[27] into a cluster. [25] successively merge the mixture component pair, merging which causes the highest change in entropy, and continue merging as long as the entropy increases. This method, abbreviated here as MMC, is implemented in the R [30] package RMIXMODCOMBI [31]. [26] developed the *directly estimated misclassification probabilities* (DEMP) algorithm to identify candidate components for merging. The author argued that the best measure of group similarity should relate to the classification probability and therefore proposed merging clusters with the highest pairwise misclassification probabilities. The DEMP+ method of [27] mimics DEMP but replaces the misclassification probabilities of DEMP with the overlap measure of [32] for Gaussian mixture components. DEMP+ uses Monte Carlo simulation to determine pairwise overlap between merged components and uses thresholds on the maximum pairwise overlap to determine termination. The sliding threshold was empirically determined by dimension, with higher dimensions requiring lower thresholds.

The MMC, DEMP and DEMP+ algorithms all rely on Gaussian mixture MBC which, while offering a principled approach to the partitioning of observations into groups with ellipsoidal structure, is demanding in CPU time and perhaps unnecessary to use when the objective is simply to find the most appropriate grouping with no particular dogma regarding shape or structure and where using k -means as a starting point for an initial clustering may be a fairly plausible but faster alternative. Perhaps recognizing this aspect, [27] contended that DEMP+ can be applied to k -means output by assuming equal mixing proportions and homogeneous spherical dispersions in the mixture model. The basis for this assertion is the framing of the k -means algorithm of [21] as a Classification Expectation-Maximization (CEM) Algorithm (see [33] for details). But k -means clustering makes hard assignments of each observation and, indeed, most commonly-used statistical software programs, such as R [30] use the efficient [20] algorithm that handles computations quite differently and sparingly than [21]. In this vein, [28] provided the K-mH algorithm to merge poorer-separated k -means groups. Such groups are identified as per an easily-computed index that uses normal theory with spherical dispersion assumptions. The K-mH algorithm has a large number of settings and parameters: using default values and rules-of-thumb provided by the authors, we have found that this method performs well in many datasets but not as well in many others. Therefore, it would be worth investigating other syncytial clustering algorithms that use k -means groupings for clustering efficiency while also reducing the need to tune multiple parameter settings.

A separate issue is the impact of Gaussian mixture model assumptions in methods such as DEMP+ when applied to regular-structured groups found using, say, the multivariate t -mixture or other appropriate models [34]. A nonparametric method not taking recourse to such distributional assumptions would be desirable in addressing this shortcoming. This paper therefore proposes the Kernel-estimated Nonparamet-

ric Overlap-Based Syncytial Clustering (KNOB-SynC) algorithm that successively merges groups from a well-optimized k -means solution until all group pairs have similar overlap or until some objective and nonparametric data-driven cluster overlap measure vanishes or is no longer reduced. This measure is calibrated through the generalized overlap [35]–[37] calculated using kernel estimators of the cumulative distribution function (CDF) developed in Section II. Our algorithm is illustrated and comprehensively evaluated in Section III. Although motivated using k -means, the method is general enough to apply to the output of other clustering algorithms: indeed, in Section IV, we show an example with groups obtained using t -mixture modeling to determine the kinds of gamma ray bursts in space. Section IV also applies our methodology to identify the types of activation in a functional Magnetic Resonance Imaging (fMRI) study. The paper concludes with some discussion. We also have an appendix providing detailed graphical illustrations of experimental performance in two-dimensional (2D) datasets.

II. METHODOLOGICAL DEVELOPMENT

A. Problem Setup

Let $\Xi = \{\mathbf{X}_1, \mathbf{X}_2, \dots, \mathbf{X}_n\}$ be a random sample of n p -dimensional observations, with each

$$\mathbf{X}_i \sim \sum_{c=1}^C \zeta_{ic} f_c(\mathbf{x}), \quad (1)$$

where C is the number of groups, $\zeta_{ic} = \mathcal{I}_{(\mathbf{X}_i \in \mathcal{C}_c)}$ with $\mathcal{I}_{(\mathcal{Z})} = 1$ if \mathcal{Z} holds, 0 otherwise, $f_c(\mathbf{x})$ is the cluster-specific density of an observation in the c th cluster and \mathcal{C}_c is the set of observations in the sample from that group. Our objective is to estimate ζ_{ic} s (equivalently, \mathcal{C}_c s) for each $c = 1, 2, \dots, C$ with C possibly unknown. We also assume that for each $c = 1, 2, \dots, C$, the density $f_c(\mathbf{x})$ for any $\mathbf{X}_i \in \mathcal{C}_c$ (*i.e.* $\zeta_{ic} = 1$) can be further described by

$$f_c(\mathbf{x}) = \sum_{k=1}^{k_c} \zeta_{ik}^{\mathcal{C}_c} h(\|\mathbf{x} - \boldsymbol{\mu}_k^{\mathcal{C}_c}\|), \quad (2)$$

where $h(\cdot)$ is defined on the positive half of the real line so that $h(\|\mathbf{x}\|)$ is a zero-centered density in \mathbb{R}^p with spherical level hyper-surfaces. This means that each group in the dataset can be further decomposed into multiple homogeneous spherically-dispersed subgroups. Thus, we can model $\mathbf{X}_i \in \Xi$ as $\mathbf{X}_i \sim \sum_{c=1}^C \sum_{k=1}^{k_c} \zeta_{ik}^{\mathcal{C}_c} h(\|\mathbf{x} - \boldsymbol{\mu}_k^{\mathcal{C}_c}\|)$, or equivalently as

$$\mathbf{X}_i \sim \sum_{k=1}^K \zeta_{ik}^{\circ} h(\|\mathbf{x} - \boldsymbol{\mu}_k^{\circ}\|), \quad (3)$$

where ζ_{ik}° s and $\boldsymbol{\mu}_k^{\circ}$ s are respectively the collection of all the $\zeta_{ik}^{\mathcal{C}_c}$ s and all the $\boldsymbol{\mu}_k^{\mathcal{C}_c}$ s. Note that $\sum_{c=1}^C \sum_{k=1}^{k_c} \zeta_{ik}^{\mathcal{C}_c} = K$ (which is also unknown). The reformulation of the density of \mathbf{X}_i as (3) means that the k -means algorithm [15], [20], [21] can be employed along with methods such as the Jump statistic [38] to obtain a first-pass clustering of the data where the dataset is partitioned into an estimated number (\hat{K}) of homogeneous spherically-dispersed groups. Our proposal in this section is to develop methods for identifying the supersets of these k -means-obtained (homogeneous spherical) groups to obtain the clusters $\{\mathcal{C}_c; c = 1, 2, \dots, C\}$ with C also requiring to be estimated. These supersets will reveal the general-shaped clustering structure in the data.

From the K -groups solution, define the i th residual ($i = 1, 2, \dots, n$) as

$$\hat{\boldsymbol{\epsilon}}_i = \mathbf{X}_i - \sum_{k=1}^{\hat{K}} \boldsymbol{\mu}_k^{\circ} \hat{\zeta}_{ik}^{\circ}. \quad (4)$$

From (4), we obtain the normed residuals, that is, $\hat{\Psi}_i = \sqrt{\hat{\boldsymbol{\epsilon}}_i^T \hat{\boldsymbol{\epsilon}}_i} = \|\mathbf{X}_i - \sum_{k=1}^{\hat{K}} \hat{\zeta}_{ik}^{\circ} \hat{\boldsymbol{\mu}}_k^{\circ}\|$ for $i = 1, \dots, n; k = 1, \dots, \hat{K}$. These $\hat{\Psi}_1, \dots, \hat{\Psi}_n$ may be viewed as a random sample with density function $h(\cdot)$ and CDF $H(\cdot)$

and having support in $[0, \infty)$. We now provide methods for estimating $H(\cdot)$ under assumptions of a smooth CDF.

B. Smooth estimation of the CDF of the normed residuals

We first introduce a smooth estimator for an univariate CDF $H(y)$. Let Y_1, Y_2, \dots, Y_n be a random sample having CDF $H(\cdot)$ and probability density function (PDF) $h(\cdot)$. The most common and natural estimator is the empirical CDF (ECDF) defined as

$$\hat{H}_n(y) = \frac{1}{n} \sum_{i=1}^n \mathbb{1}(Y_i \leq y). \quad (5)$$

It is easy to see that $\hat{H}_n(y)$ is an unbiased estimator of $H(y)$, that is, $\mathbb{E}[\hat{H}_n(y)] = H(y)$. Further, it converges almost surely to the true CDF $H(\cdot)$. However, the ECDF is a step function for any n and so is not necessarily appropriate for a smooth continuous CDF, even though it is a smooth function in the limit as $n \rightarrow \infty$ [39]. An alternative *kernel estimator* [39]–[42] for $H(\cdot)$ replaces the indicator function in (5) by a smooth function. Strictly speaking, kernel estimation is most often employed in the context of the nonparametric estimation of densities [39] but it can also be extended for smooth estimation of the CDF by integrating over the domain of the kernel. Let $G(y) = \int_{-\infty}^y K(u)du$ be the CDF of a kernel function $K(\cdot)$. The kernel CDF estimator is then defined as

$$\hat{H}_b(y) = \frac{1}{n} \sum_{i=1}^n G\left(\frac{y - Y_i}{b}\right), \quad (6)$$

where b is the *bandwidth* or the *smoothing parameter*. Equation (6) makes the popular assumption of a symmetric kernel, the most common examples of which are the Gaussian and Epanechnikov [43]–[45] kernels. However, using a symmetric kernel when the support of the distribution is not on the entire real line (as is the case with our normed residuals) causes weights to be assigned outside the domain of the observations, resulting in boundary bias [46]. So [47] proposed replacing the symmetric kernel in (6) with an asymmetric kernel, based on the gamma density, that behaves similarly as the Gaussian kernel and has a similar rate of convergence in terms of the mean squared error. However, [47]’s estimator is not a valid density for finite sample sizes [48] so we consider the Reciprocal Inverse Gaussian (RIG) kernel density estimator [49]

$$\hat{h}_b(y) = \frac{1}{n} \sum_{i=1}^n K(Y_i; y, b), \quad (7)$$

with $K(Y_i; y, b) = \frac{1}{\sqrt{2\pi b Y_i}} \exp\{-\frac{1}{2b Y_i}[Y_i - (y - b)]^2\}$. Let $G(Y_i; y, b) = \int_0^y K(Y_i; t, b)dt$. Then integrating $\hat{h}_b(y)$ with respect to y yields the smooth CDF estimator

$$\hat{H}_b(y) = \frac{1}{n} \sum_{i=1}^n G(Y_i; y, b) = \frac{1}{n} \sum_{i=1}^n \left[\Phi\left(\frac{Y_i + b}{\sqrt{Y_i b}}\right) - \Phi\left(\frac{Y_i - (y - b)}{\sqrt{Y_i b}}\right) \right], \quad (8)$$

where $\Phi(\cdot)$ is the standard Gaussian CDF. An added benefit of using the RIG kernel over the gamma kernel is that the estimated CDF is in closed form and can be readily evaluated using standard software. We provide some theoretical development on the properties of the asymmetric RIG kernel CDF estimator. Before proceeding however, we revisit the definition of the Inverse Gaussian and RIG densities for the sake of completeness and to fix ideas.

Definition 1. A nonnegative random variable $U_{\mu, \lambda}$ is said to arise from the Inverse Gaussian distribution with parameters (μ, λ) if it has the density

$$r(u; \mu, \lambda) = \begin{cases} \frac{\sqrt{\lambda}}{u\sqrt{2\pi u}} \exp\left\{-\frac{\lambda}{2\mu}\left(\frac{u}{\mu} - 2 + \frac{\mu}{u}\right)\right\}, & u > 0 \\ 0 & \text{otherwise.} \end{cases} \quad (9)$$

Notationally, we write $U_{\mu,\lambda} \sim IG(\mu, \lambda)$. Also, we have $\mathbb{E}(U_{\mu,\lambda}) = \mu$ and $\mathbb{Var}(U_{\mu,\lambda}) = \mu^3/\lambda$.

Definition 2. A nonnegative random variable $V_{\mu,\lambda}$ is said to be from the Reciprocal Inverse Gaussian distribution with parameters (μ, λ) if it has the density

$$s(v; \mu, \lambda) = \begin{cases} \frac{\sqrt{\lambda}}{\sqrt{2\pi v}} \exp \left\{ -\frac{\lambda}{2\mu} \left(v\mu - 2 + \frac{1}{\mu v} \right) \right\}, & v > 0 \\ 0 & \text{otherwise.} \end{cases} \quad (10)$$

Notationally, $V_{\mu,\lambda} \sim RIG(\mu, \lambda)$. Further, $V_{\mu,\lambda}$ is equivalent in law to $1/U_{\mu,\lambda}$ where $U_{\mu,\lambda} \sim IG(\mu, \lambda)$ and $\mathbb{E}(V_{\mu,\lambda}) = 1/\mu + 1/\lambda$ while $\mathbb{Var}(V_{\mu,\lambda}) = (\lambda + 2\mu)/(\lambda^2\mu)$.

Lemma 3. Let Y_1, Y_2, \dots, Y_n be independent identically distributed nonnegative-valued random variables with CDF $H(y)$, and PDF $h(y)$ that is infinitely differentiable. Also, let $K(\cdot; t, b)$ be a RIG kernel density defined by $K(Y_i; t, b) = \phi[(Y_i - (t-b))/\sqrt{bY_i}]/\sqrt{bY_i}$ where $\phi(z)$ is the standard normal density evaluated at z . Consider estimating $H(y)$ using $\hat{H}_b(y)$ as defined in (8). Then, as $b \rightarrow 0$, $\mathbb{E}[\hat{H}_b(y)] = H(y) + b[yh'(y) - h(y)]/2 + o(b) \equiv H(y) + \mathcal{O}(b)$ and $\mathbb{Var}[\hat{H}_b(y)] \approx H(y)(1 - H(y))/n - H(y)/(2n) - H(y)\sqrt{b}/(2n\sqrt{2\pi y}) + o(\sqrt{b}) \equiv H(y)(1 - H(y))/n - H(y)/(2n) + \mathcal{O}(b)$.

Proof. We have that $\mathbb{E}[\hat{H}_b(y)] = \mathbb{E}\left(\frac{1}{n} \sum_{i=1}^n G(Y_i; y, b)\right) = \mathbb{E}(G(Y_1; y, b)) = \int_0^\infty G(t; y, b)h(t)dt = \int_0^\infty \left(\int_0^y K(t; w, b)dw\right)h(t)dt = \int_0^y \int_0^\infty K(t; w, b)h(t)dt dw = \int_0^y \mathbb{E}[h(V_{1/(w-b), 1/b})]dw$, where the random variable $V_{1/(w-b), 1/b} \sim RIG[1/(w-b), 1/b]$. The last equality holds because the inner integral $\int_0^\infty K(t; w, b)h(t)dt = \mathbb{E}[h\{V_{1/(w-b), 1/b}\}]$. Then, expanding $V_{1/(w-b), 1/b}$ around its mean w and also using $\mathbb{Var}\{V_{1/(w-b), 1/b}\} = b(w+b)$ yields

$$\begin{aligned} \int_0^y \mathbb{E}[h\{V_{1/(w-b), 1/b}\}]dt &= \int_0^y h(w)dw + \frac{1}{2} \int_0^y (bw + b^2)h''(w)dw + o(b^2) \\ &= H(y) + \frac{b}{2} \int_0^y wh''(w)dw + o(b^2) \\ &= H(y) + \frac{by}{2}h'(y) - \frac{b}{2}[h(y) - h(0)] + o(b^2) \\ &= H(y) + \frac{b}{2}[yh'(y) - h(y)] + o(b) \equiv H(y) + \mathcal{O}(b). \end{aligned} \quad (11)$$

The definition of the variance gives $\mathbb{Var}[\hat{H}_b(y)] = \mathbb{Var}[n^{-1} \sum_{i=1}^n G(Y_i; y, b)] = \frac{1}{n} \mathbb{Var}[G(Y_1; y, b)] = \frac{1}{n} \mathbb{E}[G^2(Y_1; y, b)] - \frac{1}{n} [\mathbb{E}(G(Y_1; y, b))]^2$. The second term is easily obtained from (11). It remains to derive the second moment of the estimator, $\mathbb{E}[G^2(Y_1; y, b)] = \int_0^\infty G^2(t; y, b)h(t)dt$ which can be recast as

$$\begin{aligned} \mathbb{E}[G^2(Y_1; y, b)] &= \int_0^\infty G^2(t; y, b)h(t)dt \\ &= \int_0^\infty G(t; y, b)\Phi\left(\sqrt{\frac{t}{b}} + \sqrt{\frac{b}{t}}\right)dt - \int_0^\infty G(t; y, b)F(t; b)dt \\ &= \int_0^\infty G(t; y, b)\Phi\left(\sqrt{\frac{t}{b}} + \sqrt{\frac{b}{t}}\right)dt - \int_0^y \mathbb{E}[F(V_{1/(w-b), 1/b}; y, b)]dw, \end{aligned} \quad (12)$$

where $F(t; y, b) = \Phi\left(\sqrt{t/b} + \sqrt{b/t} - y/\sqrt{tb}\right)h(t)$ using a similar random variable $V_{1/(w-b), 1/b}$ and tactics as used in the reductions leading to (11). Since $t, b > 0$, we have that $2 \leq \sqrt{t/b} + \sqrt{b/t} < \infty$ and so $\Phi(2) \leq \Phi\left(\sqrt{t/b} + \sqrt{b/t}\right) \leq 1$. Therefore, we have

$$\Phi(2) \int_0^\infty G(t; y, b)h(t)dt \leq \int_0^\infty \Phi\left(\sqrt{\frac{t}{b}} + \sqrt{\frac{b}{t}}\right)G(t; y, b)h(t)dt \leq \int_0^\infty G(t; y, b)h(t)dt.$$

But $\int_0^\infty G(t; y, b)h(t)dt \equiv \mathbb{E}[G(Y_1; y, b) = H(y) + b[yh(y) - h(y)]/2 + o(b)]$ and $\Phi(2) = 0.97725$ so that

$$\int_0^\infty \Phi \left(\sqrt{\frac{t}{b}} + \sqrt{\frac{b}{t}} \right) G(t; y, b)h(t)dt \approx H(y) + \frac{b}{2}[yh(y) - h(y)] + o(b) \quad (13)$$

For the second term in (12), expanding $V_{1/(w-b), 1/b}$ around its mean w yields

$$\begin{aligned} & \int_0^y \mathbb{E}[F(V_{1/(w-b), 1/b}; y, b)]dw \\ &= \int_0^y F(w; y, b)dw + \frac{1}{2} \int_0^y \text{Var}(V_{1/(w-b), 1/b}; y, b)F''(w; y, b)dw + o(b) \\ &= \int_0^y \Phi \left(\sqrt{w/b} + \sqrt{b/w} - y/\sqrt{wb} \right) h(w)dw + \frac{b}{2} \int_0^y (w+b)F''(w; y, b)dw + o(b) \\ &= \Phi(\sqrt{b/y})H(y) - \int_0^y \left\{ \frac{d}{dw} \Phi \left(\sqrt{w/b} + \sqrt{b/w} - y/\sqrt{wb} \right) \int h(w)dw \right\} dw \\ & \quad + \frac{b}{2} \int_0^y (w+b)F''(w; y, b)dw + o(b) \end{aligned} \quad (14)$$

The derivative in the integrand is

$$\frac{d}{dw} \Phi \left(\sqrt{w/b} + \sqrt{b/w} - y/\sqrt{wb} \right) = \left(\frac{1}{\sqrt{bw}} + \frac{y-b}{w\sqrt{bw}} \right) \phi \left(\sqrt{\frac{w}{b}} - \frac{(y-b)}{\sqrt{bw}} \right)$$

so that (14) equals $\Phi(\sqrt{b/y})H(y) + o(\sqrt{b})$. We now expand $\Phi(\sqrt{b/y})$ using a Taylor series expansion around 0 to get $\Phi(\sqrt{b/y}) = 1/2 + \sqrt{b}/(2\sqrt{2\pi y}) + \mathcal{O}(b)$. Inserting this result into (14) and combining with (13) means that (12) is $\mathbb{E}[G^2(Y_1; y, b)] = H(y)/2 - H(y)\sqrt{b}/(2\sqrt{2\pi y}) + o(\sqrt{b})$ and the approximate expressions for the variance in Lemma 3 follow. \square

Lemma 3 shows that $\hat{H}_b(y)$ has lower variance than the ECDF and has point-wise Mean Squared Error (MSE) at y that is given by $\text{MSE}[\hat{H}_b(y)] = \text{Var}[\hat{H}_b(y)] + [\text{Bias}\{\hat{H}_b(y)\}]^2$.

1) *Bandwidth selection:* [49] minimized the Mean Integrated Squared Error (MISE) to provide a rule-of-thumb bandwidth selector for the RIG kernel density estimator of the form

$$\hat{b} = \left[\frac{2 \int_0^\infty y^{-1/2} h(y) dy}{\sqrt{\pi} \int_0^\infty y^2 \{h''(y)\}^2 dy} \right]^{2/5} n^{-2/5}. \quad (15)$$

However, \hat{b} involves knowledge of the true density $h(\cdot)$ and is directly unusable. [49] proposed obtaining \hat{b} by assuming an initial parametric density, say $h(\cdot; \theta)$, for $h(\cdot)$ and estimating the parameters θ of the density from the sample. Exact derivations using a lognormal density for $h(\cdot; \theta)$ were provided [49], but this approach has been found to produce estimates \hat{b} that are biased downwards. We therefore adopt [49]'s approach but use an initial gamma density $h(y; \vartheta, \tau) = \exp(-y/\tau)y^{\vartheta-1}\tau^\vartheta/\Gamma(\vartheta)$ for $y > 0$ and zero otherwise. Under this setup, $\int_0^\infty y^{-1/2}h(y; \vartheta, \tau)dy = \Gamma(\vartheta - 1/2)\sqrt{\tau}/\Gamma(\vartheta)$ and $\int_0^\infty y^2\{h''(y; \vartheta, \tau)\}^2dy = (6\vartheta - 4)(\vartheta - 1)\Gamma(2\vartheta)/\{4^\vartheta\tau^3\Gamma^2(\vartheta)(2\vartheta - 1)\}$. Therefore, we have

$$\hat{b} = n^{-\frac{2}{5}} \left[\frac{2^{2\hat{\vartheta}+1}\hat{\tau}^{7/2}(2\hat{\vartheta} - 1)\Gamma(\hat{\vartheta} - \frac{1}{2})\Gamma(\hat{\vartheta})}{\sqrt{\pi}(6\hat{\vartheta} - 4)(\hat{\vartheta} - 1)\Gamma(2\hat{\vartheta})} \right]^{\frac{2}{5}} \quad (16)$$

with $\hat{\vartheta}$ and $\hat{\tau}$ estimated from the sample Y_1, Y_2, \dots, Y_n using, for example, the method of moments. This \hat{b} is plugged in into (8) to obtain our smoothed RIG-kernel CDF estimator.

The development of this section, when applied to the normed residuals $\hat{\Psi}_1, \hat{\Psi}_2, \dots, \hat{\Psi}_n$, yields a smooth nonparametric kernel-based estimator of their CDF. We now use this CDF in the nonparametric estimation of the overlap measure between estimated groups.

C. A nonparametric estimator of overlap between groups

Overlap between two groups is an indicator of the extent to which they are indistinguishable from each other. [32] defined the pairwise overlap of two mixture components as the sum of the misclassification probabilities $\omega_{lk} \equiv \omega_{kl} = \omega_{l|k} + \omega_{k|l}$ with

$$\omega_{l|k} = \mathbb{P}[\mathbf{X} \text{ is assigned to } \mathcal{C}_l \mid \mathbf{X} \text{ is truly in } \mathcal{C}_k]. \quad (17)$$

For any two mixture components with densities $f(\mathbf{x} \mid \boldsymbol{\theta}_k)$ and $f(\mathbf{x} \mid \boldsymbol{\theta}_l)$ and mixing proportions π_k and π_l , $\omega_{k|l} = \mathbb{P}(\pi_k f(\mathbf{x}_i \mid \boldsymbol{\theta}_k) < \pi_l f(\mathbf{x}_i \mid \boldsymbol{\theta}_l) \mid \mathbf{x}_i \in f(\mathbf{x}_i \mid \boldsymbol{\theta}_l))$, where $\boldsymbol{\theta}_k$ and $\boldsymbol{\theta}_l$ are the parameter sets associated with the k th and l th mixture component densities respectively.

[32] calculated (17) for Gaussian mixture densities, but the definition itself is general enough to include other clustering situations including those as general as when we have cluster distributions given by densities of the type in (1). For an equal-proportioned mixture of homogeneous spherical Gaussian densities, [32] showed that $\omega_{k|l} = \Phi(\|\boldsymbol{\mu}_l - \boldsymbol{\mu}_k\|/2\sigma)$ between the k th and the l th cluster where $\Phi(\cdot)$ is the standard Gaussian CDF, $\boldsymbol{\mu}_k$ and $\boldsymbol{\mu}_l$ are the k th and the l th cluster means and σ is the common (homogeneous) standard deviation for each group, estimated unbiasedly as $WSS_K/\{(n-K)p\}$ with WSS_K being the optimized value of the within-sums-of-squares (WSS) of the K -groups solution.. The sum of $\omega_{k|l}$ and $\omega_{l|k}$ reduces to $\omega_{kl} = 2\Phi(\|\boldsymbol{\mu}_l - \boldsymbol{\mu}_k\|/2\sigma)$. The k -means formulation of (3) can be viewed more generally [50] and extends beyond the case for Gaussian-distributed groups. So we develop nonparametric methods for estimating the overlap measure.

1) *Pairwise overlap between two k -means groups:* The pairwise overlap (17) between two groups can generally be calculated from $H_\Psi(\cdot)$ as

$$\omega_{l|k} = \mathbb{P}(\|\mathbf{X} - \boldsymbol{\mu}_l\| < \|\mathbf{X} - \boldsymbol{\mu}_k\| \mid \mathbf{X} \in \mathcal{C}_k) = 1 - \mathbb{P}(\Psi_k < \Psi_{l(k)}) \quad (18)$$

where Ψ_k represents the normed residual obtained from the k th group, and $\Psi_{l(k)}$ represents the normed *pseudo-residual* which we define as the residual that is obtained by subtracting the l th cluster mean $\boldsymbol{\mu}_l$ from an observation $\mathbf{X} \in \mathcal{C}_k$. Let $H_\Psi(y)$ be the RIG kernel-estimated smooth CDF obtained using the bandwidth selected as per (16). Then, $\mathbb{P}(\Psi_k < y)$ can be estimated using $\hat{H}_\Psi(y)$. However, the calculation of $\mathbb{P}(\Psi_k < \Psi_{l(k)})$ is not as straightforward. So we propose a plug-in estimator for $\mathbb{P}(\Psi_k < \Psi_{l(k)})$ of the form

$$\hat{\mathbb{P}}(\Psi_k < \Psi_{l(k)}) = \frac{1}{n_k^\circ} \sum_{i=1}^n \hat{\zeta}_{ik}^\circ \hat{H}_\Psi(\|\mathbf{X}_i - \hat{\boldsymbol{\mu}}_l^\circ\|), \quad (19)$$

where $n_k^\circ = \sum_{i=1}^n \hat{\zeta}_{ik}^\circ$. Similar estimates of $\omega_{k|l}$ and hence ω_{kl} can be obtained. We call this estimated overlap $\hat{\omega}_{kl} \equiv \hat{\omega}_{l|k}$.

2) *Pairwise overlap between two composite groups:* A composite group is one that can be further decomposed into sub-populations as described in (2). In the following, we provide methods to extend the pairwise overlap definition of (17) for such groups.

Let $\omega_{\mathcal{C}_l|\mathcal{C}_k}$ be defined as in (17) but for composite groups. That is, we use $\omega_{\mathcal{C}_l|\mathcal{C}_k}$ rather than $\omega_{l|k}$ in order to specify that the overlap measure is between two composite clusters \mathcal{C}_l and \mathcal{C}_k . Note that $\omega_{\mathcal{C}_l|\mathcal{C}_k} = 1 - \mathbb{P}[\min_{r \in \mathcal{C}_k} \|\mathbf{X} - \boldsymbol{\mu}_r\| < \min_{j \in \mathcal{C}_l} \|\mathbf{X} - \boldsymbol{\mu}_j\| \mid \mathbf{X} \in \mathcal{C}_k]$. Suppose now that $\mathcal{C}_{s \subset k}^\circ$ is the s th spherical sub-cluster of \mathcal{C}_k with mean $\boldsymbol{\mu}_s^\circ$, $s = 1, 2, \dots, |\mathcal{C}_k|$, with $|\mathcal{C}_k|$ being the number of spherical sub-clusters in \mathcal{C}_k . For practical reasons, we make the intuitive and simplifying assumption that if $\mathbf{X} \in \mathcal{C}_k$, then $\arg\min_{r \in \{1, 2, \dots, |\mathcal{C}_k|\}} \|\mathbf{X} - \boldsymbol{\mu}_r^\circ\| = s \subset k$ implies that \mathbf{X} is in the subgroup given by $\mathcal{C}_{s \subset k}$. Under this assumption,

$$\mathbb{P}\left(\min_{r \in \mathcal{C}_k} \|\mathbf{X} - \boldsymbol{\mu}_r\| \leq y \mid \mathbf{X} \in \mathcal{C}_k\right) = 1 - \mathbb{P}\left(\min_{r \in \mathcal{C}_k} \Psi_r > y\right) = 1 - [1 - \mathbb{P}(\Psi_r \leq y)]^{|\mathcal{C}_k|} \quad (20)$$

where Ψ_r is a normed residual (obtained, for instance, from the k -means solution) for the r th spherically-dispersed subgroup in the k th cluster. We use the RIG kernel distribution estimator to obtain $\mathbb{P}(\Psi_r < y)$. From (17), and using the same ideas as in (19) we get the plug-in estimator

$$\hat{\omega}_{\mathcal{C}_l|\mathcal{C}_k} = \left[1 - \frac{1}{n_c} \sum_{i=1}^{n_c} \hat{\zeta}_{ic} \hat{H}_{\Psi}(\min_{r \in \mathcal{C}_l} \|\mathbf{X}_i - \boldsymbol{\mu}_r\|) \right]^{|\mathcal{C}_k|} \quad (21)$$

and similarly for $\hat{\omega}_{\mathcal{C}_k|\mathcal{C}_l}$, from where we calculate $\hat{\omega}_{\mathcal{C}_l\mathcal{C}_k} \equiv \hat{\omega}_{\mathcal{C}_k\mathcal{C}_l} = \hat{\omega}_{\mathcal{C}_l|\mathcal{C}_k} + \hat{\omega}_{\mathcal{C}_k|\mathcal{C}_l}$. Our definitions of \mathcal{C}_k s and $\hat{\omega}_{\mathcal{C}_k\mathcal{C}_l}$ are consistent in the sense that if $\mathcal{C}_k = \{k\}$ and $\mathcal{C}_l = \{l\}$ are both k -means groups, then $\hat{\omega}_{\mathcal{C}_k\mathcal{C}_l} = \hat{\omega}_{kl}$. We use this equivalence in the description of our KNOB-SynC algorithm in Section II-D below.

3) *Summarizing overlap in a partitioning*: Our development so far has provided us with pairwise overlap measures for k -means-type (Section II-C1) and composite (Section II-C2) groups. For a K -groups (whether of the composite or k -means type) partitioning, we get $\binom{K}{2}$ pairwise overlap measures. Summarizing the pairwise overlaps is important to provide a sense of clustering complexity so [32] originally proposed two measures: $\tilde{\omega}$ (maximum of all pairwise overlaps) and $\bar{\omega}$ (average of all $\binom{K}{2}$ pairwise overlaps). For greater control, they proposed regulating both $\tilde{\omega}$ and $\bar{\omega}$ and demonstrated (see Figures 2 and 3 of [32]) the ability to summarize a wide range of cluster geometries. Recognizing, however, that controlling two measures is cumbersome, later versions of the CARP [36] and MIXSIM [37] software packages borrowed ideas from [35] to obtain the *generalized overlap* $\ddot{\omega} = (\check{\lambda}_{\Omega} - 1)/(K - 1)$ where $\check{\lambda}_{\Omega}$ is the largest eigenvalue of the (symmetric) matrix Ω of pairwise overlaps $\omega_{l,k}$ ($\omega_{\mathcal{C}_k\mathcal{C}_l}$ for composite groups) and with diagonal entries that are all 1. The generalized overlap $\ddot{\omega}$ takes values in $[0,1]$ with zero indicating perfect separation between all groups at a distributional level and 1 indicating indistinguishability between any of them. In this paper, we obtain the estimated generalized overlap $\hat{\ddot{\omega}}$ using the estimated matrix $\hat{\Omega}$ with off-diagonal entries given by the kernel-estimated pairwise overlaps $\hat{\omega}_{l,k}$ or $\hat{\omega}_{\mathcal{C}_k\mathcal{C}_l}$, depending on whether we have simple k -means-type or composite groups.

D. The KNOB-SynC Algorithm

Having provided theoretical development for the machinery that we will use, we now describe our KNOB-SynC algorithm. Our algorithm has the following phases:

- 1) *The k -means phase*: This phase finds the optimal partition best explaining the dataset in terms of homogeneous spherically-dispersed groups and has the following steps:
 - a) For each $K \in \{1, 2, \dots, K_{\max}\}$, obtain K -means partitions initialized each of nKp times with K distinct seeds randomly chosen from the dataset and run to termination. The best (in terms of value of the objective function at termination) of each set of nKp runs is our putative optimal K -means partition for that $K \in \{1, 2, \dots, K_{\max}\}$. In this paper, we use $K_{\max} = \max\{\sqrt{n}, 50\}$.
 - b) Use the easily implemented jump statistic of [38] on the optimal K -means partitions ($K \in \{1, 2, \dots, K_{\max}\}$) obtained in Step 1a to determine the optimal K . In calculating the jump statistic, we have used $y = p/2$, which has become the default in most applications. We refer to [38] for more detailed discussion on this choice of y . Denote this optimal K by \hat{K} . The corresponding \hat{K} -means solution is the optimal homogeneous spherically-dispersed partition that best explains the dataset. This concludes the k -means phase of the algorithm.
- 2) *The initial overlap calculation phase*: This phase starts with the output of Step 1 above. That is, we start with a structural definition of the dataset in terms of \hat{K} optimal homogeneous spherically-dispersed groups. Our objective here is to calculate the overlap between each of these groups using nonparametric kernel estimation methods. We proceed as follows:
 - a) For each observation $\mathbf{X}_i, i = 1, 2, \dots, n$, compute its normed residual $\Psi_i = \sqrt{\hat{\epsilon}_i' \hat{\epsilon}_i}$ where ϵ_i is as defined in (4). Also for each observation \mathbf{X}_i , obtain the normed pseudo-residual $\Psi_{i;l(k)} = \|\mathbf{X}_i - \hat{\boldsymbol{\mu}}_k\|$ for $\mathbf{X}_i \in \mathcal{C}_k$, and $l \neq k \in \{1, 2, \dots, \hat{K}\}$.

- b) Using the set of normed residuals $\{\Psi_i; i = 1, 2, \dots, n\}$, obtain its RIG-kernel estimated CDF using (6) with bandwidth determined as per (16).
 - c) For any two groups $k \neq l \in \{1, 2, \dots, \hat{K}\}$, estimate the pairwise overlap $\hat{\omega}_{lk} = \hat{\omega}_{l|k} + \hat{\omega}_{k|l}$, where $\hat{\omega}_{l|k}$ and $\hat{\omega}_{k|l}$ are calculated using (18) and (19). Thus we obtain the estimated overlap matrix $\hat{\Omega}$ (with diagonal elements all equal to unity). For clarity, we denote this overlap matrix as $\hat{\Omega}^{(1)}$ and the pairwise overlaps as $\hat{\omega}_{kl}^{(1)} \equiv \hat{\omega}_{\mathcal{C}_k \mathcal{C}_l}^{(1)}$.
 - d) From the overlap matrix $\hat{\Omega}^{(1)}$, calculate the generalized overlap $\check{\omega}$. Call it $\check{\omega}^{(1)}$.
- 3) *The merging phase*:: The merging phase is triggered only if some pairwise overlaps are more than the others (equivalently, if $\check{\omega}^{(1)} \not\approx \check{\omega}$ where $\check{\omega}$ is the maximum of the pairwise overlaps) or if the generalized overlap is not negligible, that is, if $\check{\omega}^{(1)} \not\approx 0$. (In our implementation, we assume that two overlap measures are approximately the same if they less than 10^{-5} apart.) In that case, this phase merges groups, provides pairwise overlap measures between newly-formed composite groups, the updated overlap matrix and the generalized overlap, continuing as long as the generalized overlap keeps decreasing or is not negligible. Specifically, this phase iteratively proceeds for $\ell = 1, 2, \dots$ as per the following steps:
- a) Merge the groups with the maximum overlap and every pair of groups with individual pairwise overlaps substantially larger than the generalized overlap $\check{\omega}^{(\ell)}$. That is, merge every pair of groups $\mathcal{C}_k, \mathcal{C}_l, k \neq l$ such that $\hat{\omega}_{lk}^{(\ell)} \equiv \check{\omega}^{(\ell)}$ or $\hat{\omega}_{lk}^{(\ell)} > \kappa \check{\omega}^{(\ell)}$. Call the new merged group $\mathcal{C}_{\min(k,l)}$ and decrease the label index in the groups with indices greater than $\max(k,l)$ by 1. Decrement \hat{K} by 1 for each pair merged.
 - b) Using (21), update the pairwise overlap measures that have changed as a result of the merges in Step 3a. Call the updated measures $\hat{\omega}_{\mathcal{C}_k \mathcal{C}_l}^{(\ell+1)}$. Obtain the updated overlap matrix (call it $\hat{\Omega}^{(\ell+1)}$) and calculate the updated generalized overlap $\check{\omega}^{(\ell+1)}$. Set $\ell \leftarrow \ell + 1$.
 - c) The merging phase terminates if either $\check{\omega}^{(\ell)} > \check{\omega}^{(\ell-1)}$, or $\check{\omega}^{(\ell)} \approx 0$, or $\check{\omega}^{(\ell)} \approx \check{\omega}^{(\ell)}$. The terminating \hat{K} is the estimated \hat{C} of (1).
- 4) *Final clustering solution*:: The grouping $\{\mathcal{C}_1, \mathcal{C}_2, \dots, \mathcal{C}_{\hat{C}}\}$ at the end of the merging phase is the final partition of the dataset. Thus, there is a total of \hat{C} general-shaped groups in the dataset.
- a) *Comments*:: We provide some additional discussion on KNOB-SynC and relate it to other syn-cytial clustering algorithms:
- 1) The k -means phase finds regular-structured (homogeneous spherical) groups and in this respect is similar to K-mH [28] and EAC [23]. However, note that EAC repeats k -means with fixed K several times. Unlike K-mH which uses the KL criterion [51] to determine the initial K , we use [38]’s jump statistic to decide on the initial K . We use k -means for speed and efficiency and also because it allows us to explore larger candidate values of K . The approach could very well have been used with model-based clustering algorithms that initially partitions the dataset into, for instance, multivariate- t or Gaussian groups of varying dispersions and proportions. In that case, the initial overlap calculation phase would involve spherizing the residuals before continuing on with the initial overlap calculation phase in Step 2 and subsequent phases. We visit an example of this case in Section IV-A.
 - 2) The choice of κ determines the types of composite groups that are formed. For larger values of κ , we have groups formed by merging a few pairs in each iteration while for smaller values of κ , we get many merges at a time. In the first case, we expect merging strings of clusters while in the second case, we find clusters that are irregular-shaped but less stringy. A data-driven approach to choosing κ , that we adopt, runs the algorithm with different values of $\kappa = 1, 2, 3, \infty$ (say) and to use the partitioning with the smallest terminating $\check{\omega}$ as the optimal clustering.
 - 3) As with MMC, DEMP or DEMP+, the use of cluster distributions in the overlap calculations simplifies the computational aspects of the problem: on the other hand, EAC and K-mH require cross-tabulation of the entire dataset across clusterings and is memory-intensive and not easily

applied to larger datasets.

- 4) KNOB-SynC uses analytical methods to update the overlap between composite groups, unlike DEMP+ which uses Monte Carlo simulation and therefore is slower. Further, DEMP+ uses the maximum overlap which is very sensitive to individual pairwise overlap measures while KNOB-SynC uses the generalized overlap measure [35] which provides a nonlinear summary of the individual pairwise overlap measures.
- 5) Unlike DEMP or DEMP+, the stopping criterion of KNOB-SynC is data-driven allowing for the possibility of obtaining well-separated and less well-separated partitionings as supported by the data.
- 6) The use of nonparametric methods in the overlap calculations means that a large number of methods can be used in the initial partitioning phase. The method can also potentially be modified to apply to other kinds of datasets. For instance, the initial clustering could be done for categorical datasets using k -modes [52], [53] and then inverse discrete CDF-fitting (see Chapter 3 of [54]) and copula model [55] on each cluster to obtain numerical-valued residuals for use with our overlap estimation and calculations.

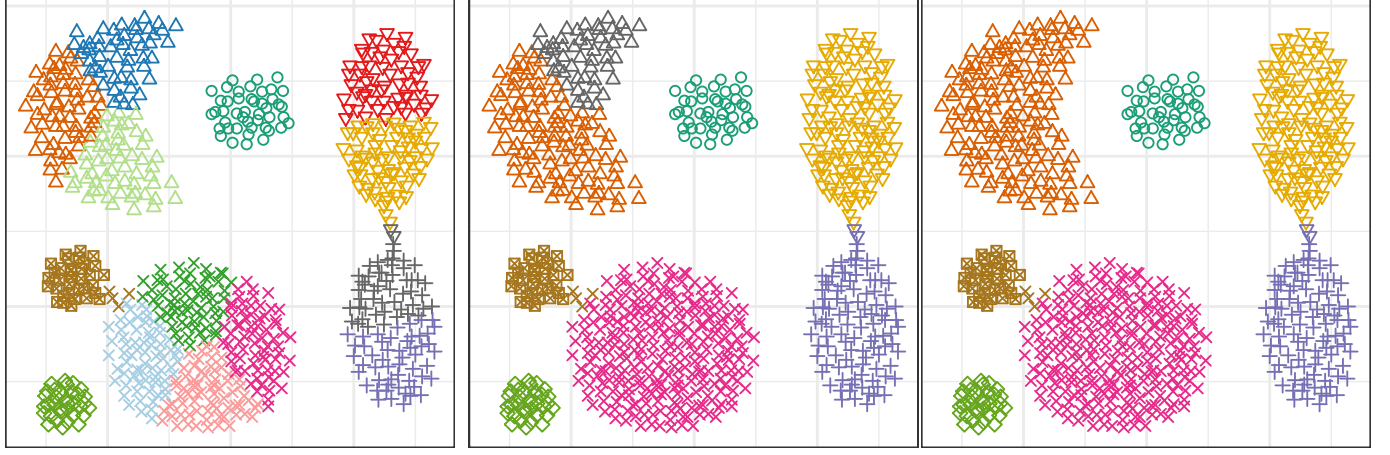
Having proposed our KNOB-SynC algorithm, we now illustrate and evaluate its performance in relation to a host of competing methods.

III. PERFORMANCE EVALUATIONS

We first illustrate the performance of KNOB-SynC on a two-dimensional *Aggregation* dataset of [56] and then follow up with more detailed performance evaluations with a large number of datasets in the literature. These datasets ranged from two to many dimensions. We compared our methods with a bunch of clustering methods. Among these were the syncytial clustering techniques of K-mH [28] using author-supplied R code, MMC [25] as implemented in the R package MIXMODCOMBI, DEMP [26] using the R package FPC and DEMP+ [27]. In addition, we also evaluated performance using EAC [23], the generalized single linkage with nearest neighbor (GSL-NN) density estimate of [29] using their supplied code from the supplementary materials of the journal website. We also used two common connectivity-based techniques of spectral and kernel k -means clustering. Both methods need the number of groups to proceed: for spectral clustering we decided on the number of groups to be the one with the highest gap in successive eigenvalues of the similarity matrix [24]. For kernel k -means, we chose K to be known at the true value: we recognize that our evaluation of kernel k -means provides this method with an unfair advantage, however, we proceed in this fashion in order to understand the best case scenario of this competing method. For all datasets and cases we evaluated performance in terms of the adjusted Rand index \mathcal{R} [57] between the true partition and the estimated final partitioning using each method. The index \mathcal{R} takes values in $(-\infty, 1]$ with values closer to 1 indicating greater similarity between partitionings and good clustering performance and conversely values substantially below 1 indicating poorer clustering performance.

A. Illustrative Example: the *Aggregation* dataset

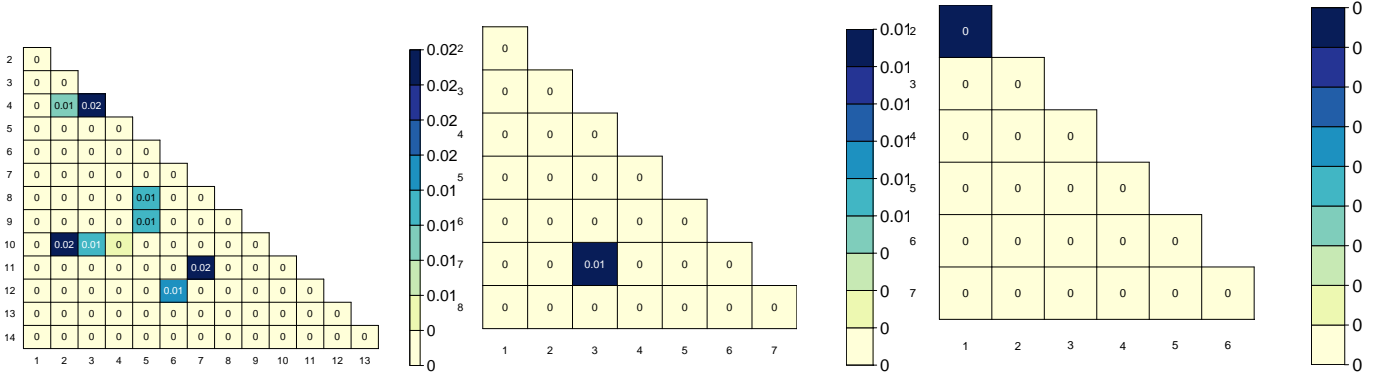
The two-dimensional *Aggregation* dataset [56] has $n = 788$ observations from $C = 7$ groups of different characteristics. Figure 1 displays the results of the different phases and iterations of KNOB-SynC and performance with competing methods. The stages of KNOB-SynC are displayed for $\kappa = 1$ which is also the one that had the lowest terminating $\hat{\omega}$ (from among $\kappa = 1, 2, 3, \infty$). In this and other similar figures in this paper, plotting color and character represent the estimated and true group identifications, respectively. The k -means phase of our algorithm identifies 14 clusters with partitioning as in Figure 1a and the initial overlap matrix $\hat{\Omega}$ of Figure 1d. The first merging phase yields the partitioning in Figure 1b with the updated $\hat{\Omega}$ of Figure 1e. The next merging phase only merges one pair of groups and is terminal, resulting in the final partitioning of the dataset as in Figure 1c. The overlap matrix (Figure 1f) indicates well-separated clusters. Only two observations are mislabeled, yielding a \mathcal{R} of 0.98 between the true and estimated classification.



(a) k -means phase end: $\hat{K} = 14$

(b) First merging phase end: $\hat{K} = 8$

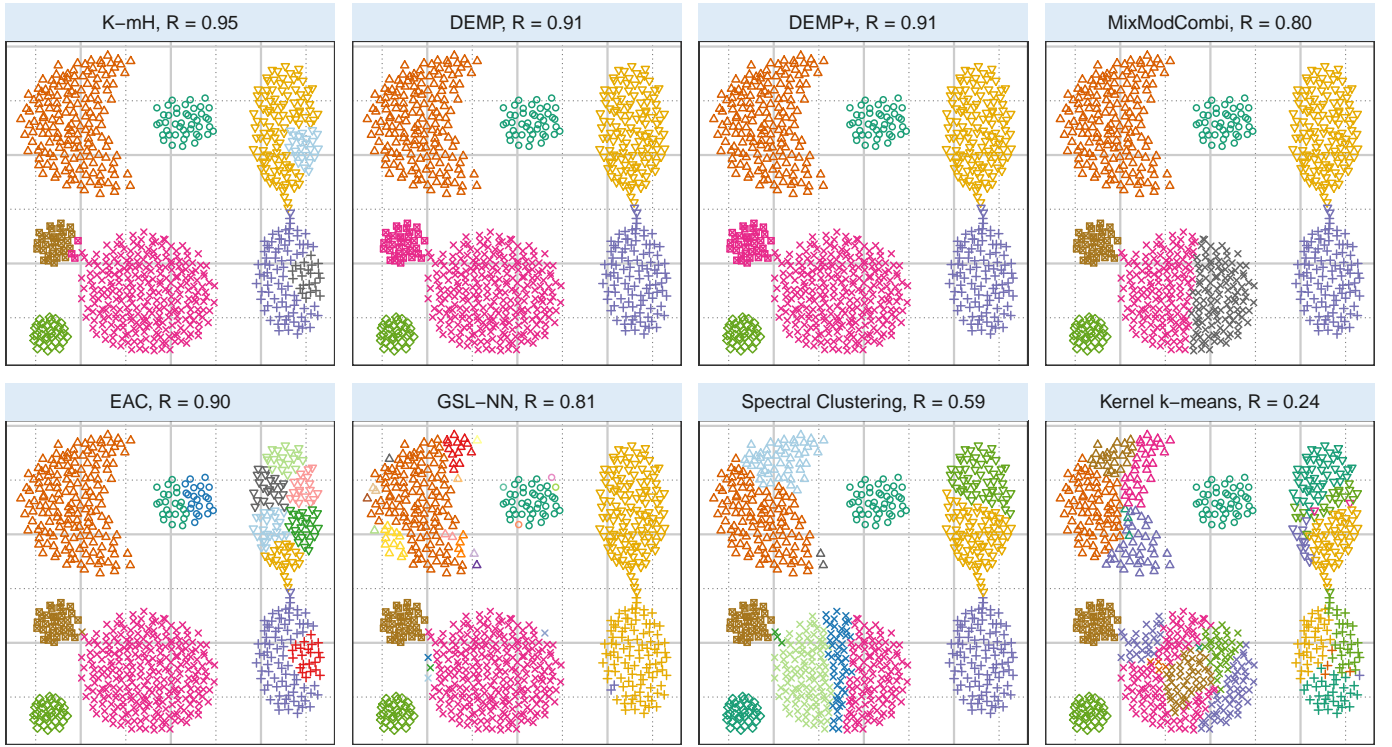
(c) Final solution: $\hat{K} = 7$



(d) k -means end: $\tilde{\omega} = 0.0013$

(e) Merging phase I: $\tilde{\omega} = 0.0008$

(f) Final solution: $\tilde{\omega} = 10^{-6}$; $\mathcal{R} = 0.98$



(g)

Fig. 1: (a)-(f) Illustrating of the KNOB-SynC algorithm on the Aggregation dataset, and (g) groups obtained using competing algorithms. In all cases, character denotes true class membership which color indicates estimated class membership.

The competing methods (Figure 1g) all perform marginally to substantially worse. K-mH is the second best performer ($\mathcal{R} = 0.95$), finding $\hat{C} = 9$ groups, but breaking the top right cluster into two and also grouping a few other stray observations. Both DEMP and DEMP+ yield the same result ($\mathcal{R} = 0.91$, $\hat{C} = 6$), but MMC has trouble with the largest group, splitting it into two, with $\mathcal{R} = 0.8$ and $\hat{C} = 8$. EAC breaks the top central and large groups on the right into many clusters, resulting in $\hat{C} = 14$ but $\mathcal{R} = 0.9$. Thus, in spite of the large number of groups, EAC is able to capture quite a bit of the complicated structure of this dataset. GSL-NN can not distinguish between the groups on the right but finds many small groups elsewhere, ending up with $\hat{C} = 12$ and $\mathcal{R} = 0.81$. Spectral clustering performs worse, finding $\hat{C} = 12$ groups with $\mathcal{R} = 0.59$. Despite being supplied the true $C = 7$, kernel k -means with $\mathcal{R} = 0.18$ is the worst performer in this example.

B. Additional 2D Experiments

1) *Experimental framework:* Figure 2 displays the 12 additional 2D datasets used to evaluate performance of KNOB-SynC and its competitors. Many of these datasets have been used by other authors to demonstrate and evaluate performance of their methods. The groups in these datasets have structure

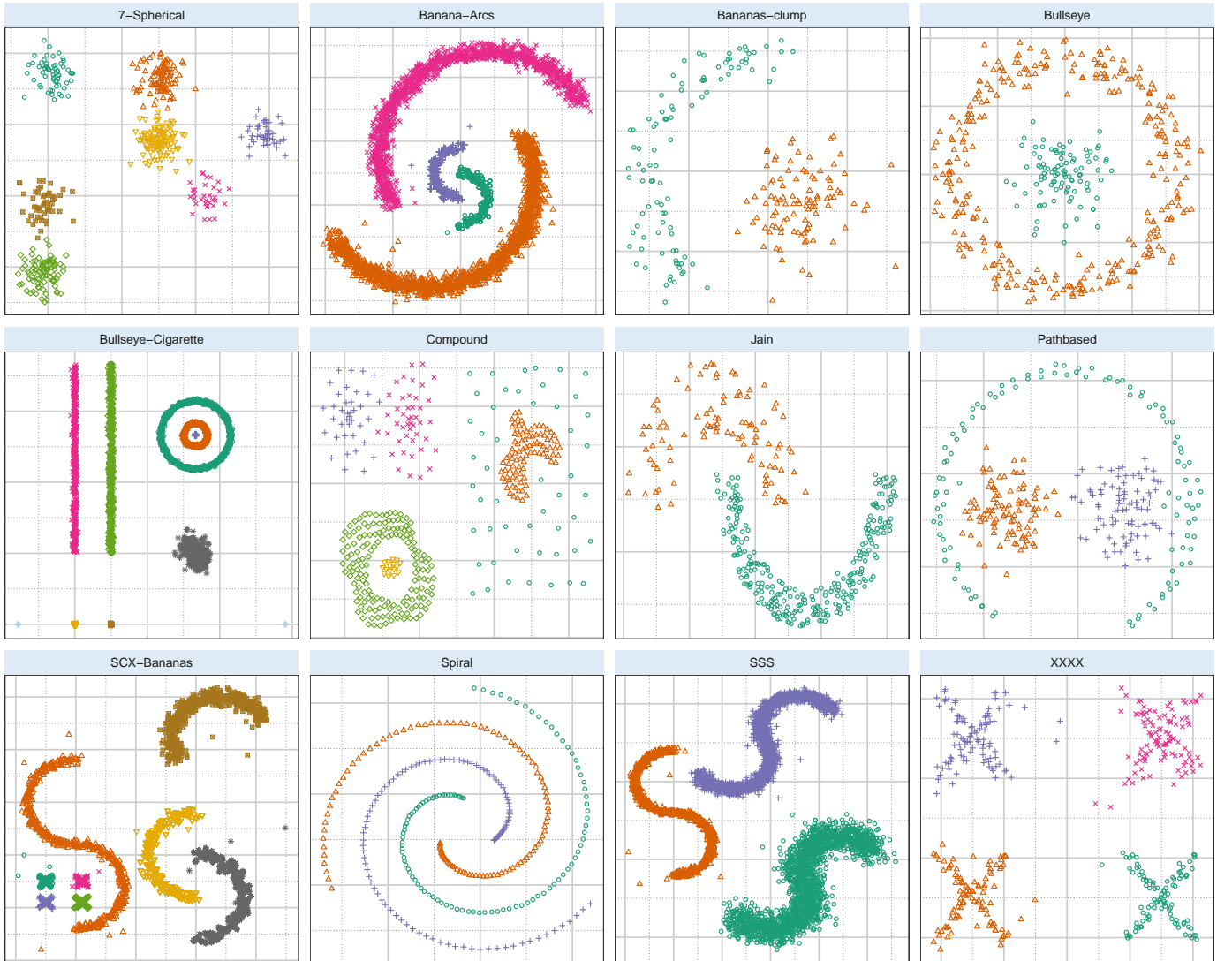


Fig. 2: Shape datasets used in the two-dimensional performance evaluations.

ranging from the regular (see *e.g.*, the 7-spherically-dispersed Gaussian clusters dataset that is modeled

on a similar example in [58]) to widely-varying complexity. The *Banana Arcs* dataset has $n = 4515$ observations clumped in four banana-shaped structures arced around each other. The *Banana-clump* and *Bullseye* datasets were used in [29] and [28] – the former has 200 observations with one spherical group and another arced around it on the left like a banana, while the latter has 400 observations grouped, as its name implies, as a bullseye. The more complex-structured *Bullseye-Cigarette* dataset [28] has three concentric ringed groups, two elongated groups above two spherical groups on the left, and another group that is actually a superset of two overlapping spherical groups ($n = 3025$ and $C = 8$). The *Compound* dataset [59] is very complex-structured with $n = 399$ observations in $C = 6$ groups that are not just varied in shape, but a group that sits atop another on the right. The *Jain* dataset [60] has 373 observations in two arc-shaped clusters, one of which is dense and the other very sparsely-populated. The *Pathbased* dataset [61] has 300 observations in three groups, two of which are regular-shaped and surrounded by a widely arcing third group. The *Spiral* dataset [61] has 312 observations in three spiral groups that very difficult for standard clustering algorithms to recover. The *SSS* dataset has 5015 observations in three S-shaped groups of varying density and orientations while the *XXXX* dataset has $n = 415$ observations distributed in four cross-shaped structures in the dataset.

2) *Results*: Figure 3 and Table I summarizes the results of all the methods in the 2-dimensional experimental datasets. Detailed displays of different methods (with the exception of kernel k -means, which we skip for compactness of the figure, and also because of its need for given K) on individual

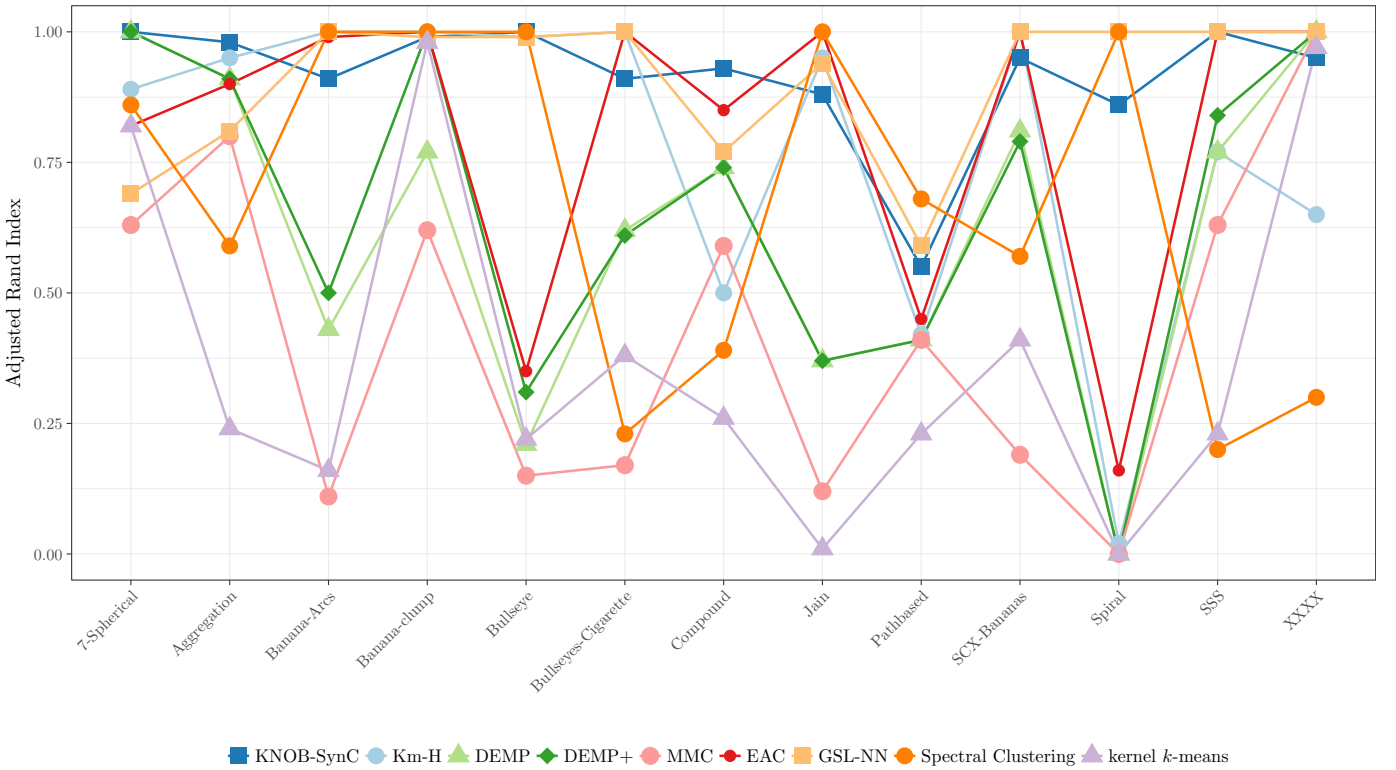


Fig. 3: Performance, in terms of the Adjusted Rand Index, of all methods on 2D datasets.

datasets are in Appendix A. The summaries indicate across-the-board good performance of KNOB-SynC, in terms of \mathcal{R} , with it being close to the top in almost all cases. In its worst case here, KNOB-SynC gets a $\mathcal{R} = 0.55$ on the *Pathbased* dataset because it terminates early (Figure 15), but here also it is the third-best performer, behind spectral clustering ($\mathcal{R} = 0.77$) and EAC ($\mathcal{R} = 0.59$). The competing syncytial clustering methods do well in some cases, but not in others where the other comparison methods perform better. Among the syncytial clustering methods, K-mH perform better than DEMP, DEMP+ and MMC whose performance can be poor in some cases (e.g., on the *Bullseye* and *Jain* and *Spiral* datasets of 11, 14 and 17, respectively). It is on these datasets that the other methods (EAC, GSL-NN,

TABLE I: Performance, in terms of \mathcal{R} and estimated \hat{C} , on 2D datasets, of competing methods: KNOB-SynC (denoted as KNS in the table), K-mH, DEMP (DM), DEMP+ (DM+), MMC, EAC, GSL-NN (GSN), spectral clustering (SpC) and kernel- k -means (k- k m). For k- k m, \hat{C} was set at the true C and not estimated. For each method, the absolute deviation of \mathcal{R} for that method from the highest \mathcal{R} for each dataset was obtained: the average and SD of these absolute deviations are also reported for each method in the last row.

Dataset (n, p, K)		KNS	K-mH	DM	DM+	MMC	EAC	GSN	SpC	k- k m
7-Spherical (500, 2, 7)	\mathcal{R}	0.98	0.89	1.00	1.00	0.63	0.82	0.69	0.86	0.82
	\hat{C}	7	10	7	7	5	9	10	7	
Aggregation (788, 2, 7)	\mathcal{R}	0.98	0.93	0.91	0.91	0.83	0.94	0.81	0.84	0.18
	\hat{C}	7	9	6	6	5	12	11	7	
Banana-arcs (4515, 2, 4)	\mathcal{R}	0.91	1.00	0.5	0.54	0.13	1.00	1.00	1.00	0.16
	\hat{C}	5	1	15	10	39	6	6	4	
Banana-clump (200, 2, 2)	\mathcal{R}	0.99	1.00	0.77	1.00	0.62	1.00	0.99	1.00	0.98
	\hat{C}	3	2	3	2	5	2	3	3	
Bullseye (400, 2, 2)	\mathcal{R}	1.00	0.92	0.21	0.31	0.20	0.51	0.99	1.00	0.22
	\hat{C}	2	2	7	5	10	5	3	2	
Bullseye-cig (3025, 2, 8)	\mathcal{R}	0.99	0.62	0.64	0.37	1.00	1.00	0.38	0.82	0.38
	\hat{C}	7	6	7	7	5	9	15	7	
Compound (399, 2, 6)	\mathcal{R}	0.93	0.5	0.74	0.74	0.59	0.85	0.77	0.39	0.26
	\hat{C}	19	12	3	3	3	8	14	16	
Jain (373, 2, 2)	\mathcal{R}	0.88	0.95	0.37	0.37	0.12	1.00	0.94	1.00	0.01
	\hat{C}	16	3	6	6	11	2	4	2	
Pathbased (300, 2, 3)	\mathcal{R}	0.55	0.42	0.41	0.41	0.41	0.45	0.59	0.77	0.23
	\hat{C}	21	2	2	2	3	15	6	3	
SCX-Bananas (3420, 2, 8)	\mathcal{R}	0.95	1	0.81	0.79	0.19	1.00	1.00	0.57	0.41
	\hat{C}	8	8	7	9	39	8	8	4	
Spiral (312, 2, 3)	\mathcal{R}	0.86	0.01	0.00	0.00	0.00	0.18	1.00	1.00	0
	\hat{C}	3	2	1	1	1	9	3	3	
SSS (5015, 2, 3)	\mathcal{R}	1.00	0.77	0.77	0.84	0.63	1.00	1.00	0.2	0.23
	\hat{C}	3	5	5	4	27	4	3	19	
XXXX (415, 2, 4)	\mathcal{R}	0.95	0.65	1.00	1.00	1.00	1.00	1.00	0.30	0.97
	\hat{C}	10	6	4	4	4	4	4	20	
$\bar{\mathcal{D}}$		0.052	0.118	0.348	0.316	0.552	0.159	0.062	0.29	0.591
\mathcal{D}_σ		0.055	0.280	0.310	0.311	0.331	0.273	0.097	0.326	0.331

Spectral clustering) do better. The performance of kernel- k -means is varied, even with known true number of groups, being very good sometimes (*e.g.*, in the `Bananas-clump` dataset of Figure 10) but very poor in cases (*e.g.*, as seen before in the `Aggregation` dataset) where every other method does well. We quantify performance of each method against its competitors in terms of its average deviation from the best performer. Specifically, for each dataset, we compute the difference in \mathcal{R} of a method from that of the best performer for that dataset. We call these deviations. The average deviation ($\bar{\mathcal{D}}$) of a method over all datasets is an overall indicator of its performance. Table I provides $\bar{\mathcal{D}}$ and the standard deviation (\mathcal{D}_σ) of the differences. On the average, KNOB-SynC is the best performer (also having the lowest \mathcal{D}_σ) followed by GSL-NN, K-mH and EAC. We surmise that KNOB-SynC does well across the different kinds of datasets because of its ability by construction to merge many or few components at a time, with the exact choice and termination completely data-driven and objective and determined by the distinctiveness of the resulting partitioning as measured by $\hat{\omega}$.

C. Higher-Dimensional Datasets

We also studied the performance of KNOB-SynC and its competitors in higher-dimensional datasets. These datasets are modest to higher-dimensional and range in size from over 173 to 10993. For the higher-

dimensional datasets (Acute Lymphoblastic Leukemia and Zipcode digits), we found that all methods other than GSL-NN perform better when used on the first few (m) kernel principal components (KPCs) rather than on the raw data. For these methods and these datasets therefore, we used the first m KPCs of each dataset with m chosen as the first time after which increases in the eigenvalues corresponding to the successive KPCs are below 0.5%. GSL-NN was evaluated on the original datasets. We describe the datasets and performance in the next sections and summarize performance on all the datasets in Section III-C10.

1) *Simplex-7 Gaussian Clusters*: This dataset, from [29], is of Gaussian realizations of size 50, 60, 70, 80, 90, 100 and 110 each from seven clusters with means set at the vertices of the seven-dimensional unit simplex and homogeneous spherical dispersions with common standard deviation of 0.25 in each dimension. Like the 7-Spherical dataset, it is an example of a case where standard methods such as k -means or Gaussian-mixture-model-based clustering should be adequate. Therefore it is a test of whether our algorithm and its competitors are able to refrain from identifying spurious complexity. All methods identify seven groups and have good clustering performance. In particular, the syncytial methods have very good performance ($\mathcal{R} = 0.97$) and only marginally better than the others (then $0.92 \leq \mathcal{R} \leq 0.94$).

2) *E. coli Protein Localization*: The *E. coli* dataset, publicly available from the University of California Irvine’s Machine Learning Repository (UCIMLR) [62], concerns identification of protein localization sites for the *E. coli* bacteria, an important early step for finding remedies [63]. There are eight protein localization sites: cytoplasm, inner membrane without signal sequence, periplasm, or inner membrane with an uncleavable signal sequence, outer membrane, outer membrane lipoprotein, inner membrane lipoprotein or inner membrane with a cleavable signal sequence. Identifying these sites is an important early step for finding remedies [63]. Each protein sequence has a number of numerical attributes – see [64] for a listing and their detailed description. Two attributes are binary, but 326 of the 336 sequences have common values for these attributes. We restrict our investigation to these sequences and drop these two attributes from our list of variables. These 326 sequences have no representation from the inner membrane or outer membrane lipoproteins. Additionally, we also drop two sequences because they are the lone representatives from the inner membrane with cleavable sequence site [65]. Therefore we have $n = 324$ observations from $C = 5$

TABLE II: Confusion matrix of the KNOB-SynC grouping against the true for the *E. coli* dataset.

	1	2	3	4	5	6	7	8	9
cytoplasm	138	0	0	4	0	0	0	0	1
inner membrane, no signal sequence	7	62	0	0	0	3	3	1	0
inner membrane, uncleavable signal sequence	1	32	0	0	0	0	0	1	0
outer membrane	0	0	17	2	0	0	0	0	0
periplasm	3	1	2	38	8	0	0	0	0

true classes. For this example KNOB-SynC identifies $\hat{C} = 9$ groups. Table II presents the confusion matrix containing the number of cases a protein from a localization site was assigned to KNOB-SynC group. Ignoring stray assignments, the sites are fairly well-defined in the first four groups, with $\mathcal{R} = 0.72$. Uncleavable signal sequences from the inner membrane site are difficult to distinguish from those that are also from there but have no signal sequence. Sequences from the other sites are better-clarified. Among the alternative methods, EAC does slightly better ($\mathcal{R} = 0.77$) but identifies 10 groups. The remaining methods all do slightly to substantially worse. DEMP, DEMP+ and K-mH each identify four groups but with $\mathcal{R} \in [0.63, 0.78]$. K-mH finds only two groups ($\mathcal{R} = 0.41$) while the rest find more groups but disagree more strongly with the true localization. Thus EAC and KNOB-SynC are the top two performers for this dataset.

3) *Wine Recognition*: The wine recognition dataset [66], [67] also obtainable from the UCIMLR contains $p = 13$ measurements on $n = 178$ wine samples that are obtained from its chemical analysis. There are 59, 71 and 48 wines of the Barolo, Grignolino and Barbera cultivars, respectively, so $C = 3$. KNOB-SynC is a middling performer for this dataset, finding $\hat{C} = 24$ groups with a clustering performance of $\mathcal{R} = 0.55$. All 48 members of the largest identified group are from the Barola cultivar while all 42 members of the second group are from the Grignolino cultivar. The third group has two Grignolino

wines and 35 wines from the Barbera cultivar. Thus, there is fairly good definition among these groups. However, there are a large number of very small groups also identified which explains the reduced clustering performance. Among competitors, only MMC ($\mathcal{R} = 0.67; \hat{C} = 5$), K-mH ($\mathcal{R} = 0.62, \hat{C} = 6$) and EAC ($\mathcal{R} = 0.60; \hat{C} = 9$) do better and the others do marginally to moderately worse.

4) *Olive Oils*: The olive oils dataset [68], [69] has measurements on 8 chemical components for 572 samples of olive oil taken from 9 different areas in Italy which are from three regions: Sardinia and Northern and Southern Italy. This is an interesting dataset with sub-classes (areas) inside classes (regions). Indeed, [28] were able to identify sub-groups within the regions with one misclassification but not the areas ($\mathcal{R} = 0.67, \hat{C} = 11$; we however found $\mathcal{R} = 0.56, \hat{C} = 8$ using the authors’ supplied code): they surmised that it may be more possible to identify characteristics of olive oils based on regions based on physical geography rather than areas based on political geography. We therefore analyze performance on this dataset in terms of how both regions and areas are recovered. KNOB-SynC identifies four regions with oils from the Sardinian and Northern regions being correctly classified into the first two groups. The Southern region oils are split into our two remaining groups, one containing all but 2 of the 25 North Apulian samples and 6 of the 36 Sicilian samples, and the other group containing all the Southern oils. In terms of clustering performance, KNOB-SynC gets $\mathcal{R} = 0.55$ when compared to the true areal grouping but $\mathcal{R} = 0.87$ when compared to the true regional grouping. For this dataset DEMP ($\mathcal{R} = 0.85; \hat{C} = 7$), DEMP+ ($\mathcal{R} = 0.82; \hat{C} = 12$) and MMC ($\mathcal{R} = 0.66; \hat{C} = 11$) are the top three performers when comparing with the true areal grouping: all other methods do worse than KNOB-SynC. However, in terms of comparisons with the true regional grouping, KNOB-SynC is by far the best performer. Overall, this clustering performance of KNOB-SynC marginally trumps the performance of DEMP for the areal grouping and so can be considered to be the most accurate in uncovering the group structure in the dataset.

5) *Yeast Protein Localization*: The yeast protein localization dataset [70] also obtained from the UCIMLR was used by [27] to illustrate the application of DEMP+. This dataset is on the localization of the proteins in yeast into one of ($C = 10$) sites and has two attributes (presence of “HDEL” substring and peroxisomal targeting signal in the C-term) that are essentially binary and trinary, respectively. Following [27], we drop these variables and use the other $p = 6$ variables, namely signal sequence recognition score based on (a) McGeoch’s and (b) von Heijne’s methods, (c) ALOM membrane spanning region prediction score, and discriminant analysis scores of the amino acid content of (d) N-terminal region (20 residues long) of mitochondrial and non-mitochondrial proteins and (e) vacuolar and extracellular proteins and (f) discriminant scores of nuclear localization signals of nuclear and non-nuclear proteins. For this dataset, all methods perform poorly. KNOB-SynC ($\mathcal{R} = 0.13; \hat{C} = 6$) is the best performer, with the others being essentially random allocations. Surprisingly, DEMP+ does very poorly. ([27] only used the first five variables in his illustration and DEMP+’s clustering quality was not reported: we found no appreciable performance even in that case). It appears therefore that groups may be difficult to find in the yeast protein localization dataset in a completely unsupervised framework.

6) *Image Segmentation*: The image segmentation dataset, also available from the UCIMLR, is on 19 attributes of the scene in each 3×3 image, as per hand-drawn classification into BRICKFACE, CEMENT, FOLIAGE, GRASS, PATH, SKY and WINDOW. (Thus $C = 7$.) We combine the training and test datasets to obtain 330 instances of each scene, so $n = 2310$. There is a lot of redundancy in the attributes so we reduce the dataset to eight principal components (PCs) that explains at least 99.9% of the total variability in the dataset. We use PCs computed on the correlation matrix because of the wide range in scales for the 19 attributes. The KNOB-SynC solution found $\hat{C} = 12$ clusters, with $\mathcal{R} = 0.55$. The confusion matrix (Table III) indicates that the SKY scene is perfectly identified while GRASS and, to a lesser extent, PATH and CEMENT, are fairly well-identified. EAC does slightly better than KNOB-SynC ($\mathcal{R} = 0.59$) but identifies 40 groups. Inspection of that grouping indicates many small groups but also difficulty in separating FOLIAGE and WINDOW, placing them together in one group. Further, BRICKFACE is split into five groups, four of which are predominantly of this kind, but the fifth group is unable to distinguish 146 observations of BRICKFACE from 32, 52 and 62 observations of CEMENT, FOLIAGE

TABLE III: Confusion matrix of the KNOB-SynC grouping against the true for the Image dataset.

	1	2	3	4	5	6	7	8	9	10	11	12
BRICKFACE	330	0	0	0	0	0	0	0	0	0	0	0
CEMENT	42	257	0	4	0	27	0	0	0	0	0	0
FOLIAGE	300	5	0	0	0	5	2	7	3	1	3	4
GRASS	1	0	327	0	0	2	0	0	0	0	0	0
PATH	0	0	0	269	0	61	0	0	0	0	0	0
SKY	0	0	0	0	330	0	0	0	0	0	0	0
WINDOW	309	13	0	0	0	8	0	0	0	0	0	0

and WINDOW, respectively.

7) *Acute Lymphoblastic Leukemia*: The Acute Lymphoblastic Leukemia (ALL) training dataset of [71] was used by [29] to illustrate GSL-NN in a high-dimensional small sample size framework. We used the standardized dataset in [29] that measured the oligonucleotide expression levels of the 1000 highest-varying genes in 215 patients suffering from one of seven leukemia subtypes, namely, T-ALL, E2A-PBX1, BCR-ABL, TEL-AML1, MLL rearrangement, Hyperploid > 50 chromosomes, or an unknown category labeled OTHER. Some subtypes have very few cases: for instance, only 9, 14 and 18 patients are of type BCR-ABL, MLL and E2A-PBX1, respectively. For this dataset, we used $m = 42$ KPCs for all methods but for GSL-NN. KNOB-SynC identifies $\hat{C} = 16$ groups, with $\mathcal{R} = 0.59$. Table IV presents

TABLE IV: Confusion matrix of the KNOB-SynC grouping against the true for the ALL dataset.

	1	2	3	4	5	6	7	8	9	10	11	12	13	14	15	16
Hyperdiploid > 50	35	0	0	0	2	0	0	2	1	1	0	0	0	1	0	0
E2A-PBX1	0	17	0	0	0	0	0	0	0	0	1	1	0	0	0	0
OTHERS	0	0	51	0	0	0	0	0	0	1	1	0	0	0	0	0
BCR-ABL	2	0	0	3	4	0	0	0	0	0	0	0	0	0	0	0
TEL-AML1	7	2	6	0	12	8	0	1	5	0	0	1	9	1	0	0
MLL	0	4	0	0	0	10	0	0	0	0	0	0	0	0	0	0
T-ALL	0	0	0	0	0	0	24	0	0	0	0	0	0	0	3	1

the confusion matrix containing the number of cases a patient of a leukemia subtype was assigned to a KNOB-SynC group. Three of the syncytial clustered groups have only one observation, another two have two observations and three other groups have three observations. The TEL-AML1 and BCR-ABL leukemia subtypes are scattered over multiple groups, but the other subtypes are fairly well-identified and largely get assigned to their own KNOB-SynC groups. The alternative methods perform mildly to substantially worse. GSL-NN, spectral clustering, EAC and kernel k -means ($C = 7$, given) have similar performance while K-mH, DEMP and DEMP+ do poorly in accurately finding structure in the dataset.

8) *Zipcode images*: The zipcode images [29] dataset consists of $n = 2000$ 16×16 images of hand-written Hindu-Arabic numerals and is our second higher-dimensional example. As in the ALL dataset of Section III-C7, we normalized the observations to have zero mean and variance so that the Euclidean distance between any two normalized images is negatively and linearly related to the correlation between their pixels. We extracted and used the first $m = 33$ KPCs for all algorithms but GSL-NN. KNOB-SynC identified 9 groups and had the best clustering performance ($\mathcal{R} = 0.76$). Figure 4 displays the 2000 digits with color scale for each of the 9 KNOB-SynC groups. While outliers abound in almost all groups, there is good agreement with 0, 1, 2, the leaner 8s and, less-so, 3 and 6 largely correctly identified. The digit 2 is placed in two groups, of the leaner and the rounded versions, respectively. The group where 3 predominates also has some 5's and 8's but the categorization makes visual sense. Another group is composed largely of 4s, 7s and 9s but the placement also appears visually explainable. Clearer and straighter 7s and 9s are placed in a separate group. Our partitioning finds it harder to distinguish between 5 and 6 but here also the commonality of the strokes in the digits assigned to this group explains this categorization. The alternative methods all perform moderately ($\mathcal{R} = 0.55$, $\hat{C} = 22$ for K-mH; $\mathcal{R} = 0.54$, $\hat{C} = 5$ and 7, respectively for both spectral clustering and GSL-NN) to substantially worse. Thus KNOB-SynC is the

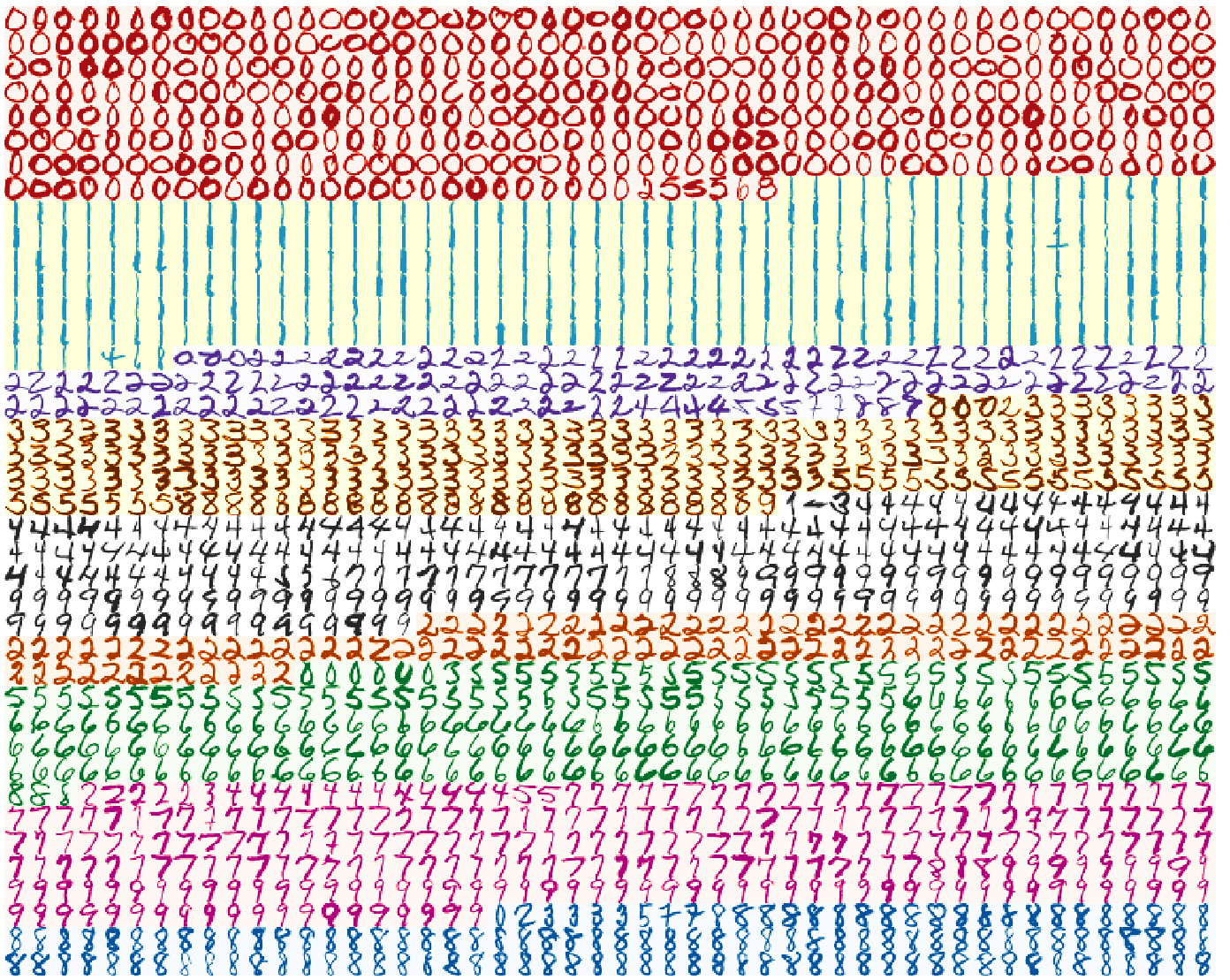


Fig. 4: KNOB-SynC groups, with colormap indicating group, of the Zipcode dataset.

best performer for this dataset and also provides interpretable results. We comment that the application of all methods to this dataset has been entirely unsupervised: methodologies that also account for spatial context and pixel neighborhood have the potential to further improve classification but are outside the purview of this paper.

- 9) *Handwritten Pen-digits*: The Handwritten Pen-digits dataset [72], [73] available at the UCI MLR

TABLE V: Confusion matrix for the Handwritten Pen-digits dataset.

	1	2	3	4	5	6	7	8	9	10	11	12	13
0	1119	1	2	0	17	0	2	0	0	0	1	0	1
1	0	640	359	138	2	0	0	3	1	0	0	0	0
2	0	2	1140	1	0	0	0	0	1	0	0	0	0
3	0	14	2	1036	1	0	2	0	0	0	0	0	0
4	0	12	1	3	1113	0	14	1	0	0	0	0	0
5	0	0	0	246	1	624	181	0	0	2	1	0	0
6	0	0	2	1	2	1	0	1050	0	0	0	0	0
7	0	144	8	0	0	0	0	0	911	0	0	79	0
8	2	0	70	33	0	2	0	0	4	372	524	48	0
9	0	9	0	311	13	0	697	0	0	0	1	0	24

is a larger dataset that measured 16 attributes from 250 handwritten samples of 30 writers. (There are

$n = 10,992$ records because eight samples are unavailable.) Following [28], we used the first 7 principal component scores that explained 90% of the total variation in the dataset. Because of the size of the dataset, our comparisons are only with EAC and K-mH (the other methods either took a very long time or threw up errors). KNOB-SynC found 13 groups and was the best performer ($\mathcal{R} = 0.69$). It found 0, 2, 3, 4, 6 and 7 fairly well but identifying 1, 5 and 9 was more difficult (Table V). It also suggested that multiple types of 8. EAC identified the correct number of groups but performed very poorly ($\mathcal{R} = 0.1$) while K-mH identified $\hat{C} = 24$ with ($\mathcal{R} = 0.64$).

10) *Summary of Performance:* Figure 5 and Table VI summarize performance of all methods on the higher-dimensional examples. It is easy to see that KNOB-SynC is almost always among the top performers. Indeed, KNOB-SynC had the lowest average difference in \mathcal{R} from that of the best performing

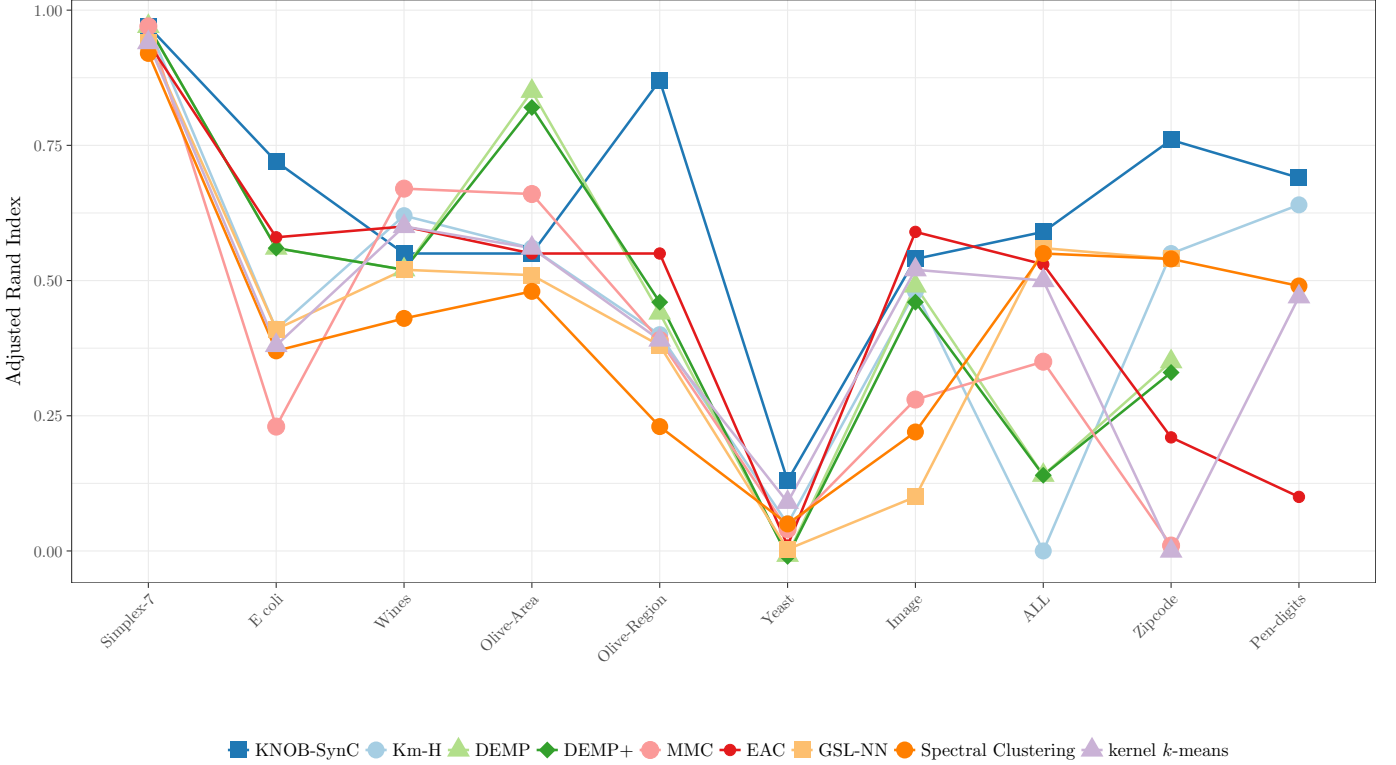


Fig. 5: Clustering performance, in terms of the Adjusted Rand Index, of KNOB-SynC and its competitors on all high-dimensional datasets.

method over all datasets (Table VI). The other methods perform similarly on the average, with EAC being the better of them, on the average.

The results of our experiments on multiple kinds of datasets in two and higher dimensions indicate good performance for the KNOB-SynC algorithm. We now apply the methodology to two real-world applications.

IV. REAL WORLD APPLICATIONS

In this section we apply KNOB-SynC to two real-world applications where the aim is to classify observations but the ground truth is not known. The first application finds the different kinds of Gamma Ray Bursts (GRBs) in astronomical datasets while the second identifies the kinds of activation detected in a fMRI experiment.

A. Determining the distinct kinds of Gamma Ray Bursts

There is tremendous interest in understanding the source and nature of Gamma Ray Bursts (GRBs) that are the brightest electromagnetic events known to occur in space [74], [75]. Many researchers [76]–

TABLE VI: Performance, in terms of \mathcal{R} and \hat{C} of all methods in the higher-dimensional datasets. Notations are as in Table VI.

Dataset (n, p, K)		KNS	K-mH	DM	DM+	MMC	EAC	GSN	SpC	k-km
Simplex-7	\mathcal{R}	0.97	0.97	0.97	0.97	0.97	0.94	0.94	0.92	0.94
(560, 7, 7)	\hat{C}	7	7	7	7	7	6	7	7	
E.coli	\mathcal{R}	0.72	0.63	0.70	0.68	0.59	0.77	0.03	0.26	0.45
(336, 7, 7)	\hat{C}	9	4	4	4	8	10	16	15	
Wines	\mathcal{R}	0.55	0.62	0.52	0.5	0.67	0.60	0.38	0.43	0.6
(178, 13, 3)	\hat{C}	24	6	7	7	5	9	15	7	
Olive-Area	\mathcal{R}	0.55	0.56	0.85	0.82	0.66	0.55	0.51	0.48	0.56
(572, 8, 9)	\hat{C}	4	8	7	12	11	14	5	18	
Olive-Region	\mathcal{R}	0.87	0.4	0.44	0.46	0.39	0.46	0.48	0.23	0.39
(572, 8, 3)	\hat{C}	4	8	7	12	11	14	16	18	
Yeast	\mathcal{R}	0.13	0.05	-0.008	-0.01	0.04	0.01	0.0031	0.05	0.09
(1484, 8, 10)	\hat{C}	6	7	5	5	33	38	33	39	
Image	\mathcal{R}	0.54	0.48	0.49	0.46	0.28	0.59	0.10	0.22	0.52
(2310, 19, 7)	\hat{C}	12	17	18	17	46	40	48	45	
ALL	\mathcal{R}	0.59	0.19	0.14	0.14	0.35	0.53	0.54	0.55	0.5
(215, 1000, 7)	\hat{C}	16	18	6	6	9	9	5	12	
Zipcode	\mathcal{R}	0.76	0.55	0.35	0.33	0.01	0.21	0.54	0.54	0.00
(2000, 256, 10)	\hat{C}	9	22	36	33	1	45	7	5	
Pendigits	\mathcal{R}	0.69	0.64	-	-	-	0.10	-	0.59	0.47
(10992, 16, 10)	\hat{C}	13	24	-	-	-	10	-	17	
\mathcal{D}		0.05	0.23	0.20	0.21	0.28	0.18	0.24	0.26	0.24
\mathcal{D}_σ		0.1	0.20	0.18	0.17	0.25	0.18	0.18	0.20	0.25

[78] have hypothesized that GRBs are of several kinds, but the exact number and descriptive properties of these groups is an area of active research and investigation. Most analyses traditionally focused on univariate and bivariate statistical and descriptive methods for classification and found two groups but other authors [74], [79] have found three different kinds of GRBs when using more variables in the clustering. Recent careful analysis [80], [81] has conclusively established five ellipsoidally-shaped groups in the GRB dataset obtained from the most recent Burst and Transient Source Experiment (BATSE) 4Br catalog. Indeed, [81] established that all nine fields of the BATSE 4Br catalog have important clustering information as per methods developed in [82]. These nine fields are the two duration variables (time by which 50% and 90% of the flux arrive), the four time-integrated fluences in the 20-50, 50-100, 100-300, and > 300 keV spectral channels, and the (three) measurements on peak fluxes in time bins of 64, 256 and 1024 milliseconds. The authors used multivariate t -mixtures model-based clustering (t -MMBC) on the logarithm of the measurements and Bayesian Information Criterion [83] for model selection to arrive at their result of five ellipsoidally-shaped groups. In terms of the properties of the astrophysical classification scheme pioneered by [79] and that uses duration, total fluence and spectrum, these five groups were categorized as long/intermediate/intermediate, short/faint/intermediate, short/faint/soft, long/bright/hard and long/intermediate hard. Figure 6(a) illustrates the five groups found using a parallel coordinates plot.

The astrophysical community has long been divided on whether there are two or three kinds of GRBs. While [81] conclusively established the presence of five ellipsoidally-dispersed groups, one aspect not studied by the authors was if these five clusters were sub-groups of a more complicated grouping structure and if in reality there were fewer (say, one, two, three or four) underlying syncytial groups that might provide support for the long-held belief in the astrophysical community. Our KNOB-SynC algorithm is fully objective and data-driven in determining the number of such groups, so it provides us with an important tool for determining such structure. We start here with the five ellipsoidal groups. This example also illustrates KNOB-SynC in a case where we use t -MMBC solutions instead of k -means ones. The k -means phase of Step 1 of the algorithm in Section II-D is replaced by t -MMBC and the clustered

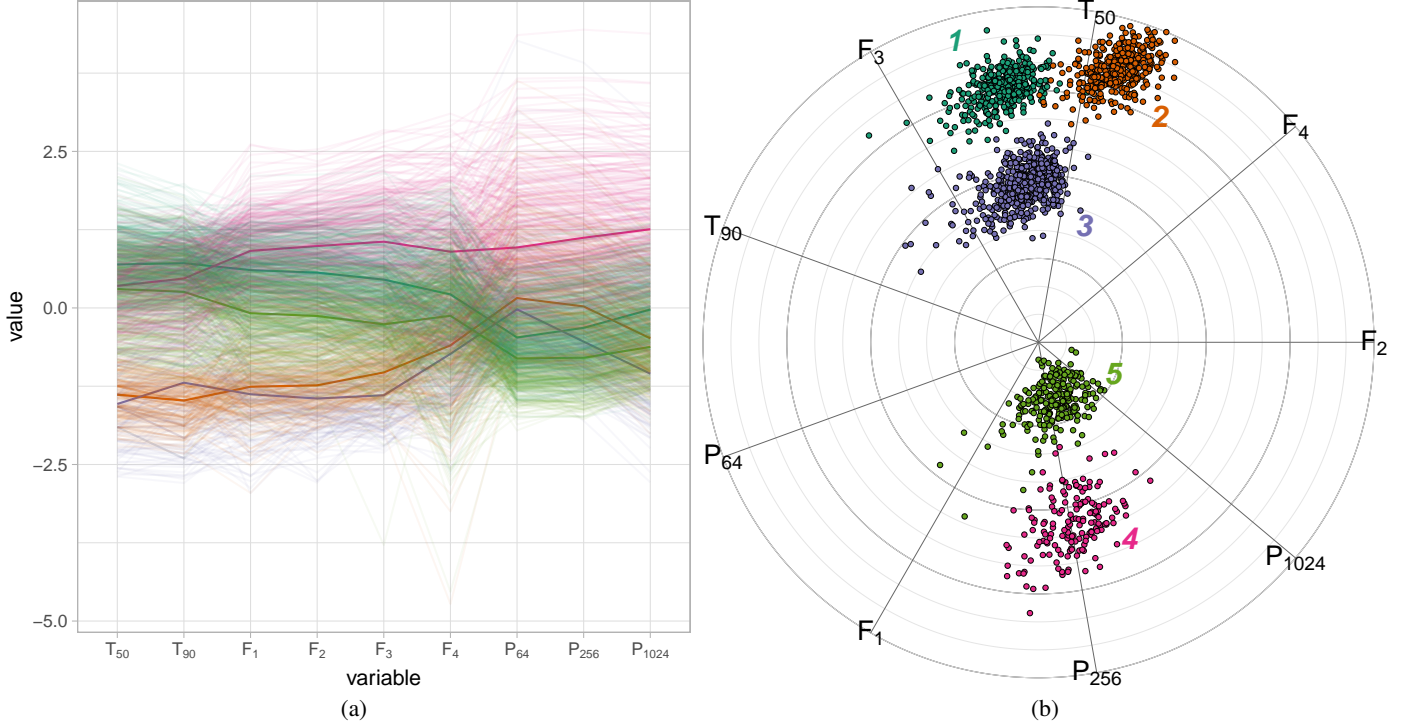


Fig. 6: (a) Parallel coordinate plot of the GRB observations using the group information as found by t -MMBC. The medians for each group are also highlighted by means of the parallel coordinates plot. (b) Standardized two-dimensional radial visualization plot of the grouped observations.

observations in each group have to be scaled and decorrelated before applying subsequent stages of the KNOB-SynC algorithm.

We first obtain and standardize the residuals of the five-groups t -MMBC solution. Then we proceed with the framework of the KNOB-SynC algorithm but from Step 2 onward. The initial overlap calculations of Step 2 with the five groups reveal a generalized overlap measure $\hat{\omega} = 3.56 \times 10^{-6}$ and a maximum overlap of 1.01×10^{-5} . So, the generalized overlap is not very different from the maximum overlap (and as also happens for the G7 and Simplex 7-Gaussian clusters datasets in Section III, the merging phase is not entered into and the algorithm terminates right away. The standardized 2D radial visualization plot in Figure 6(b) illustrates the distinctiveness of the groupings. Our results renders largely irrelevant the dispute in the astrophysical community and shows that there are five distinct kinds of GRBs in the BATSE 4Br catalog and these groups also happen to be ellipsoidally-dispersed.

B. Activation detection in a fMRI audio-visual task experiment

Our final application uses KNOB-SynC to identify activation in an audio-visual task experiment with data acquired using functional Magnetic Resonance Imaging (fMRI). One objective of fMRI is to determine cerebral regions that respond to a task or particular stimulus [84]–[87]. A typical approach relates, after correction and processing, the observed Blood Oxygen Level Dependent (BOLD) time course sequence at each image voxel to the expected BOLD response [88]–[90] by fitting a general linear model [91] and obtaining a test statistic (often a t -statistic) that tests for significance at that voxel. Thresholding methods [92], [93] are often used on these t -statistics to determine activation. Attempts to use clustering algorithms have been made, but [94] found that despite the advantages of speed and simplicity, k -means is not, in general, a good performer because it fits “data idiosyncracies” and pathologies. We therefore explore if KNOB-SynC can improve the k -means clustering solution.

We used the dataset originally from [95] but made available by [96] as DATA6 to illustrate the features of the Analysis of Functional Neuroimaging (AFNI) software. Here, a subject was presented with audiovisual speech in both auditory and visual formats, but in two situations: in the first audio-reliable case, the subject could clearly hear the spoken word but had a blurred visual of the female speaker, while the second visual-reliable case was when subject could clearly see the female speaker vocalizing the word but with degraded audio. Of interest is to identify the cerebral regions that perceive auditory stimuli differently from the visual. We refer to [95] for imaging details but note that we used AFNI to fit a time series regression model with ARMA(1,1) structure at each voxel. At each of the $n = 63353$ voxels, we computed the t -statistic to test the hypothesis that the expected BOLD levels differ significantly for the auditory and visual stimuli at a voxel. Because of the large size of the dataset, we only use KNOB-SynC on these t -statistics. The k -means phase identified $K_0 = 13$ groups. The application of subsequent phases of the KNOB-SynC algorithm ended with $K = 4$ syncytial groups. Figure 7a shows the distribution of the t -statistics in each group by means of a violin plot. The largest (first) group has 61886 (97.6%) voxels

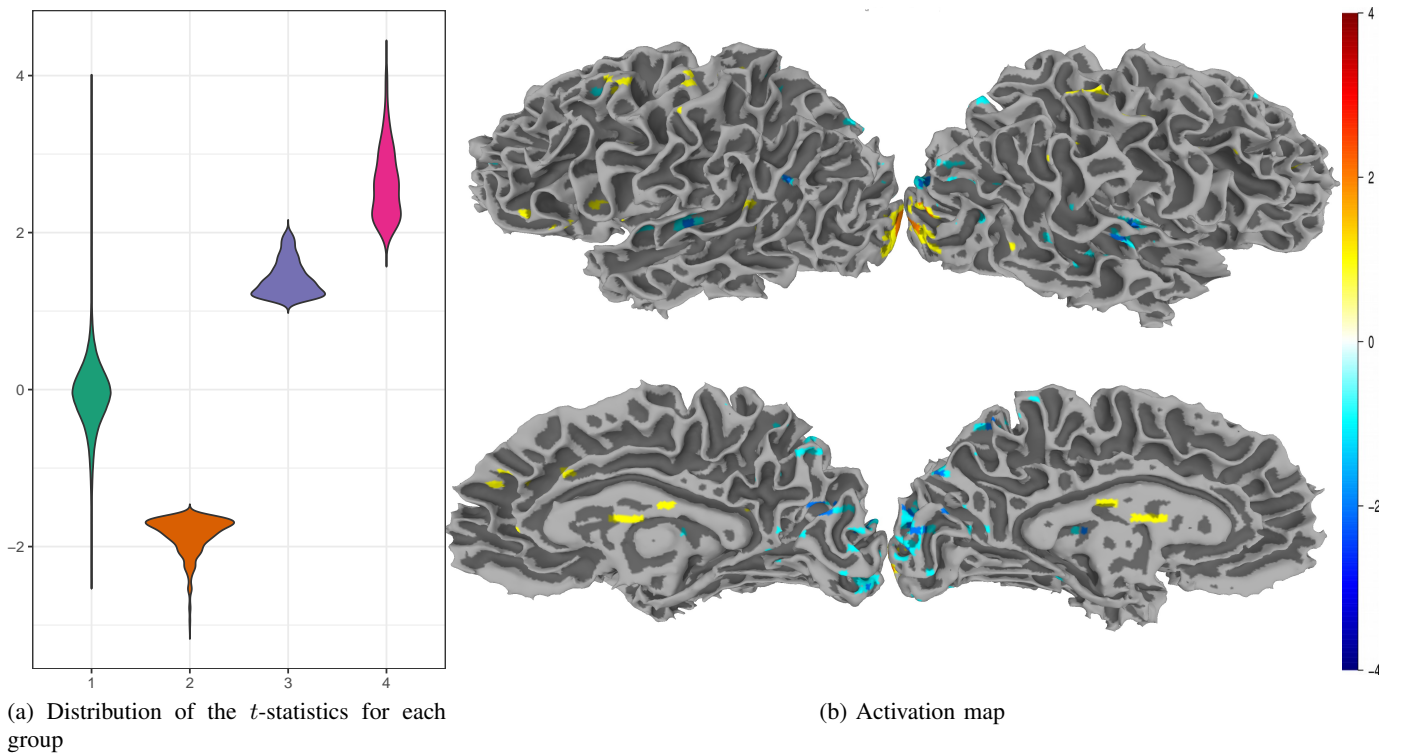


Fig. 7: Violin plots to display cluster solution using KNOB-SynC and resulting activated map.

and is the essentially the region of no activation or no difference in activation owing to either stimuli. The second group has 643 voxels and are of the regions that respond to the auditory but not the visual stimuli. The other two regions are comprised of 698 and 126 voxels and represent regions that respond to the visual but not the auditory stimuli with the smaller region responding more emphatically than the other. Figure 7b displays the t -statistics obtained at the voxels in the three activated groups. We see that the regions are in the Brodmann areas 19 (BA19) where visual associations, feature-extraction, shape recognition, attentional, and multimodal integrating functions take place. A detailed analysis of these results is outside the purview of this paper, but we note that the results are interpretable. This example illustrates the potential of KNOB-SynC to improve and refine clustering solutions making it possible, for instance, to use k -means and to alleviate some of the concerns raised in [94].

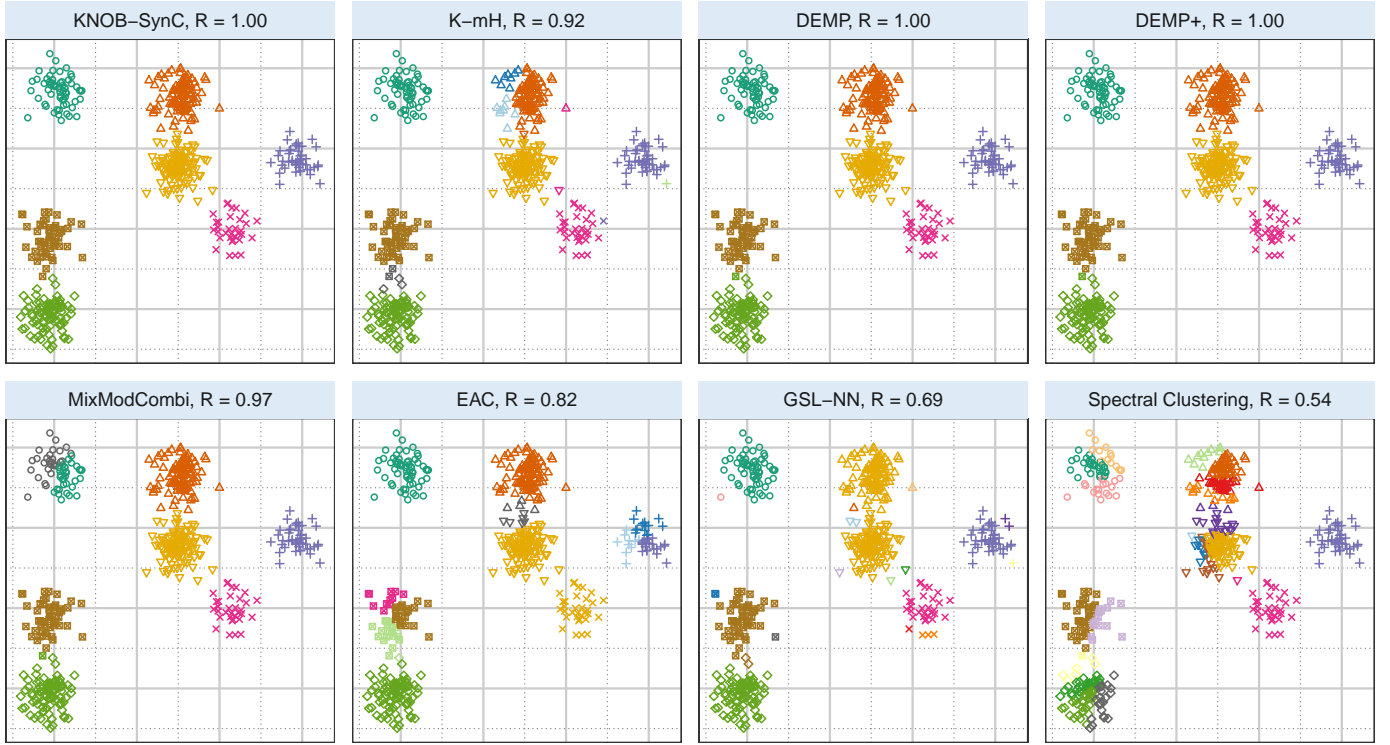


Fig. 8: Classifications obtained upon clustering the 7-Spherical dataset.

V. DISCUSSION

In this paper, we propose a syncytial clustering algorithm called KNOB-SynC that merges groups found by standard clustering algorithms, and does so in a fully data-driven and objective way. A [30] package, KNOB-SYN implementing ours and competing methods is under development and will be released soon. Our method is distribution-free and can apply to the results of many standard clustering algorithms. We use the overlap measure of [32] for merging and for decisions but use kernel-based nonparametric overlap methods to calculate this overlap. Performance is very good on experiments in datasets of many dimensions and with little to tremendous complexity, when compared against a host of other methods. Application of our methodology to GRB data provides evidence that there are five (ellipsoidally-dispersed) kinds of GRBs. Our methodology also potentially makes it possible to adapt k -means clustering on activation detection in fMRI.

This paper also developed estimation methods of the CDF using the asymmetric RIG kernel. We used the plugin-bandwidth selector that minimizes the MISE as our bandwidth choice but it would be good to have more formal methods. Further, our development in this paper provides an opportunity to develop nonparametric methods for diagnostics in clustering. For instance, our developed kernel CDF estimator could be used to determine uncertainties of k -means classifications. Thus, we see that though we have made an important contribution, there are a number of issues would benefit from further attention.

APPENDIX

This section illustrates classifications on 2D datasets obtained by KNOB-SynC, K-mH, DEMP, DEMP+, MMC (MIXMODCOMBI), EAC, GSL-NN and Spectral clustering algorithms. In all cases, plotting character and color represent the true and estimated group indicator.

REFERENCES

- [1] F. Murtagh, *Multi-dimensional clustering algorithms*. Berlin; New York: Springer-Verlag, 1985.

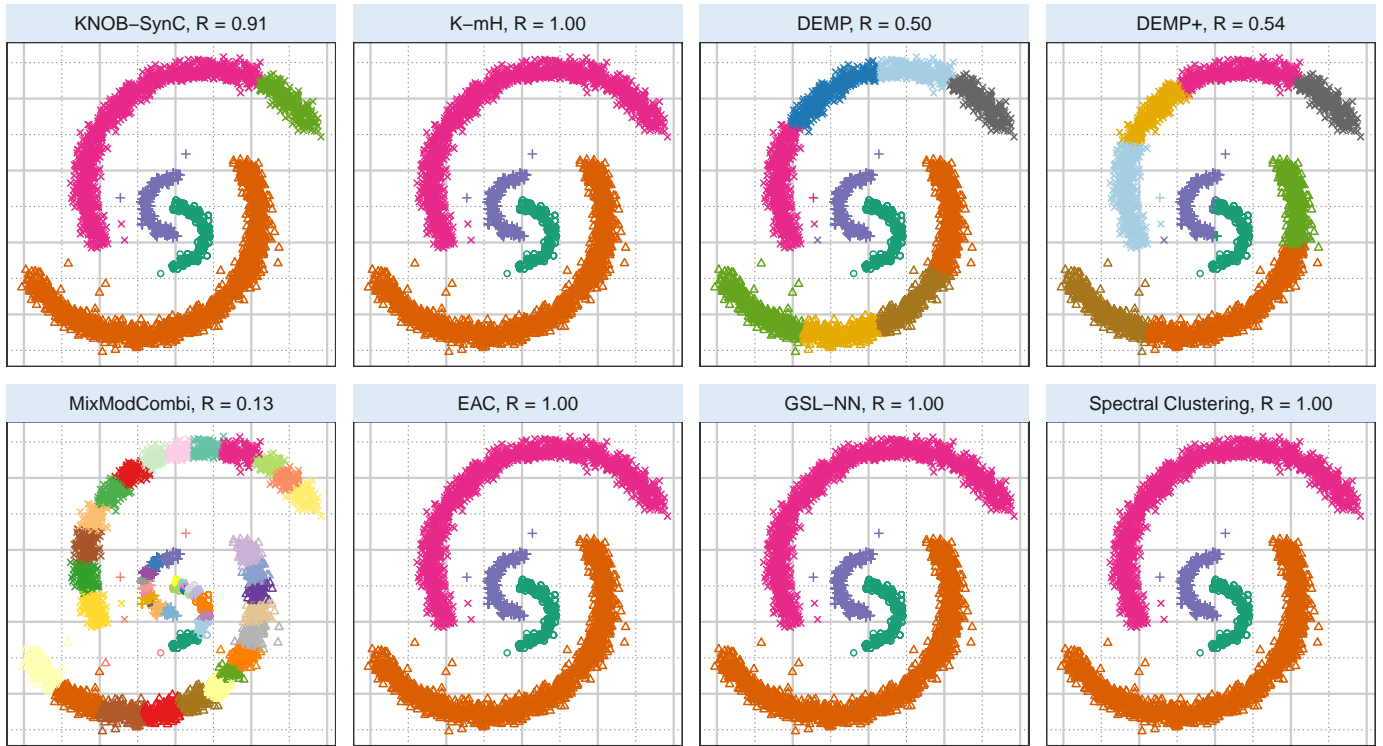


Fig. 9: Groupings obtained using the 8 algorithms on the banana-arcs dataset.

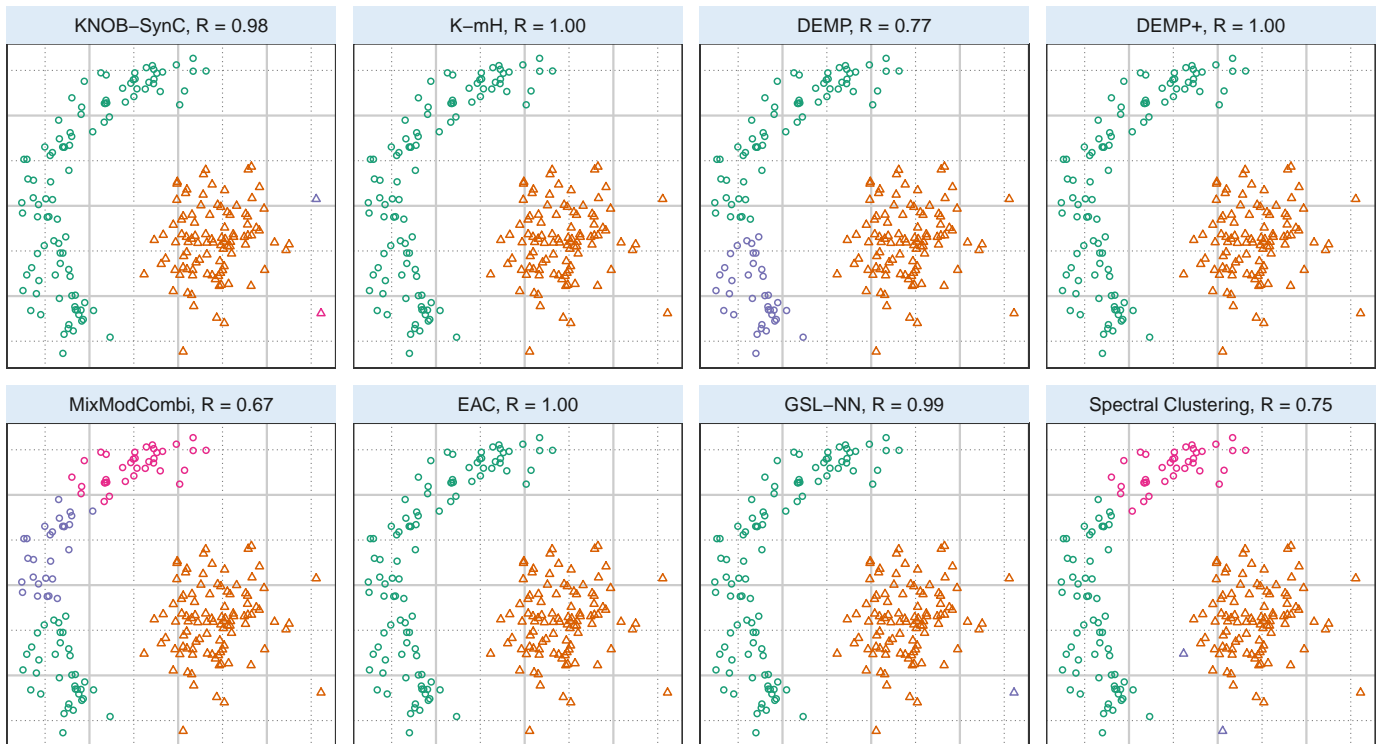


Fig. 10: Groupings obtained upon clustering the Bananas-clump dataset.

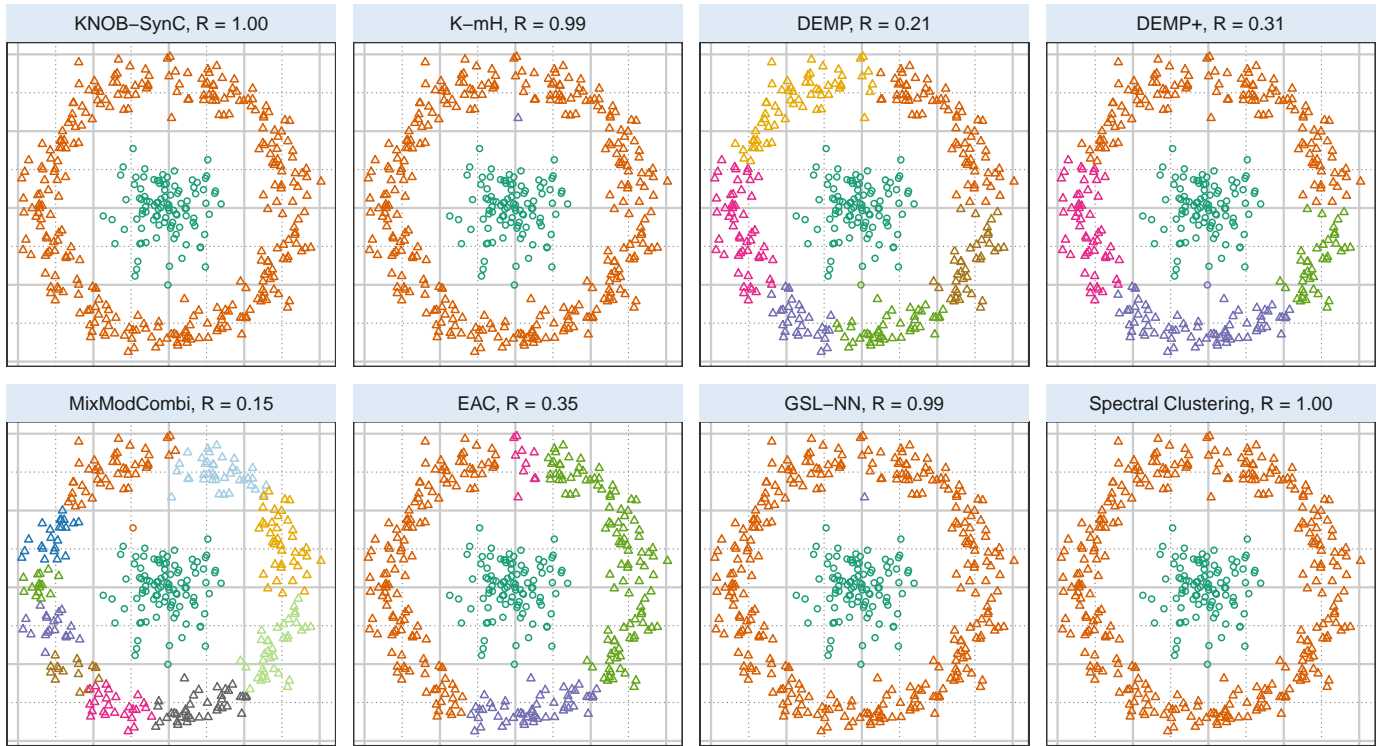


Fig. 11: Classifications obtained using the 8 algorithms on the bullseye dataset.



Fig. 12: Partitionings obtained upon clustering the Bullseye-cigarette dataset.

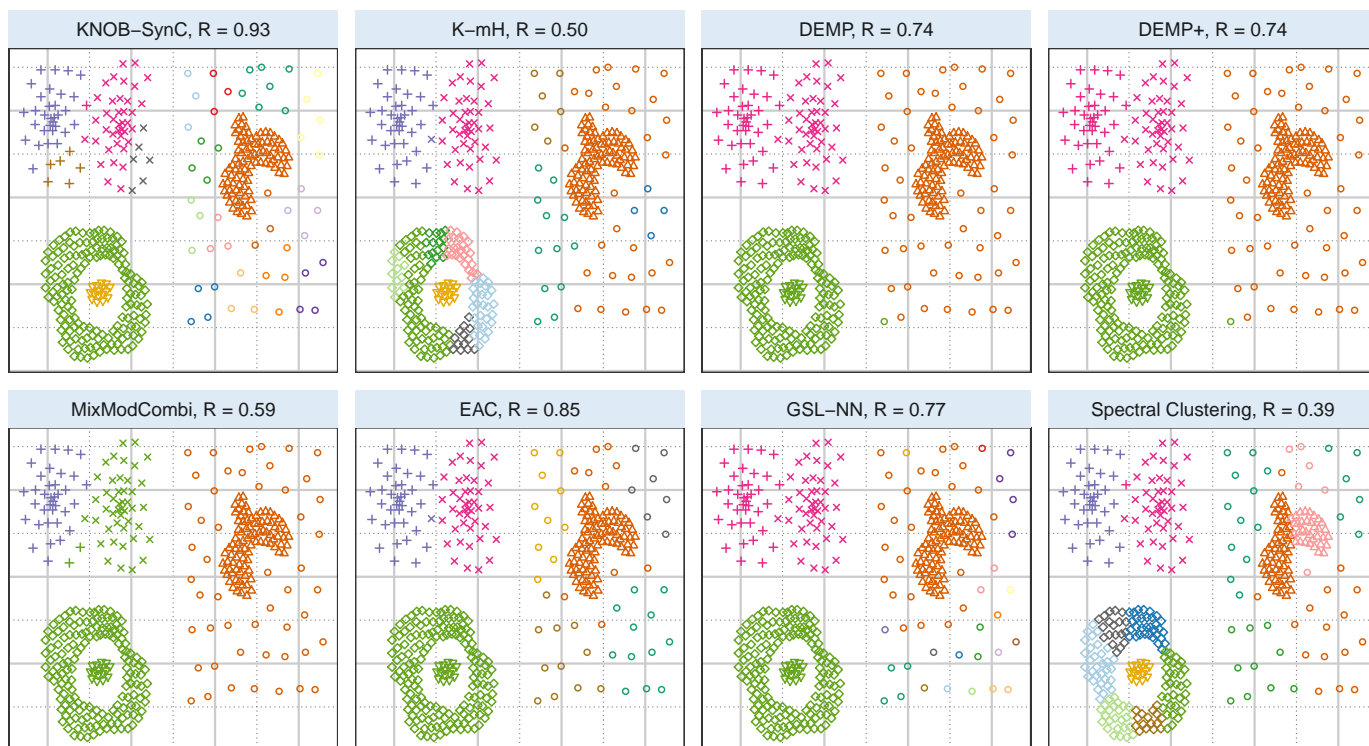


Fig. 13: Groupings obtained using the 8 algorithms on the compound dataset.

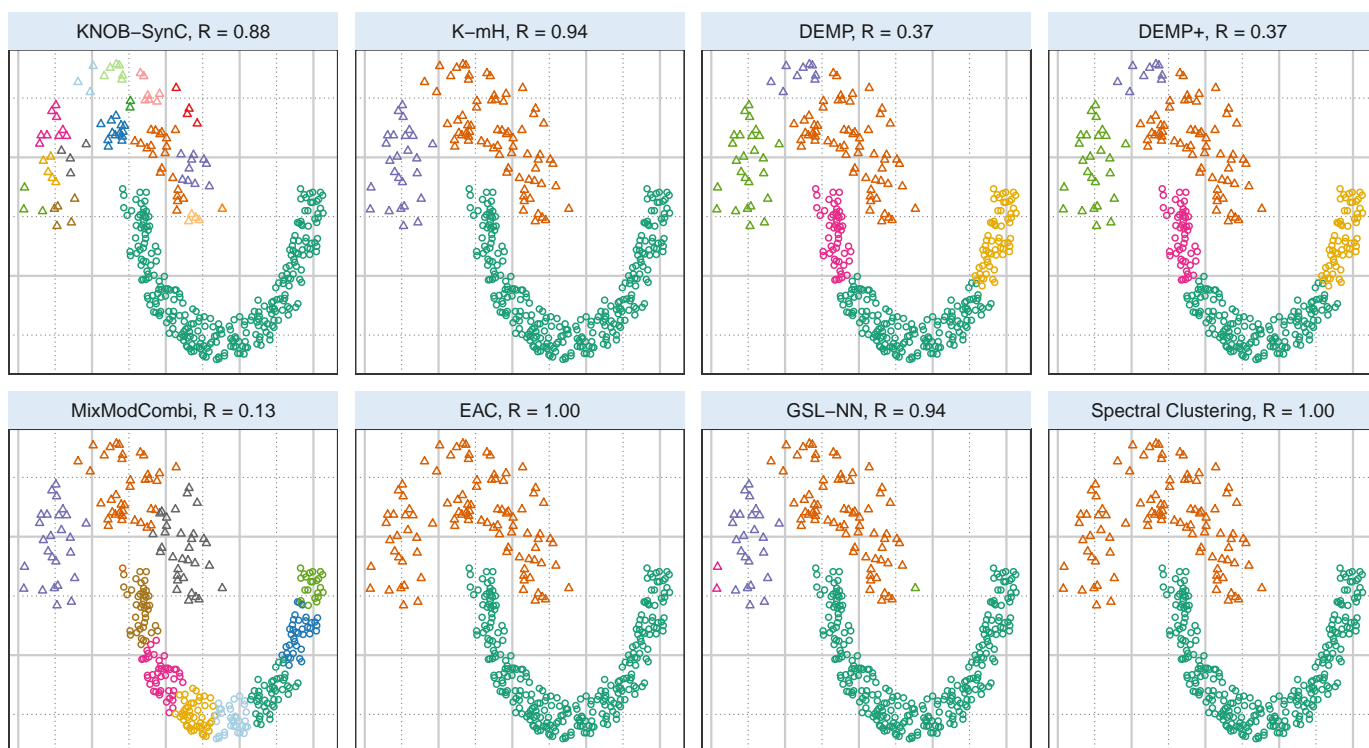


Fig. 14: Classifications obtained using the 8 algorithms clustering on the Jain dataset.

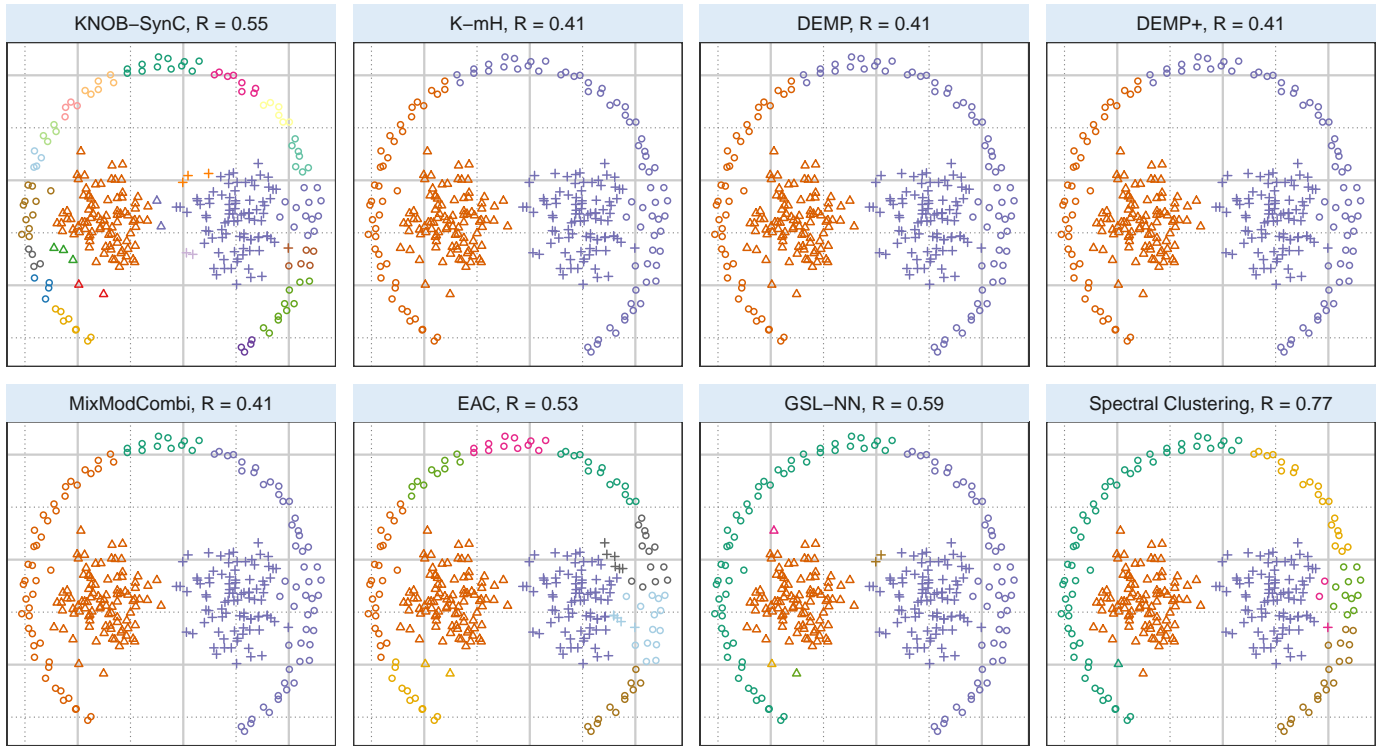


Fig. 15: Groupings obtained upon clustering the pathbased dataset.

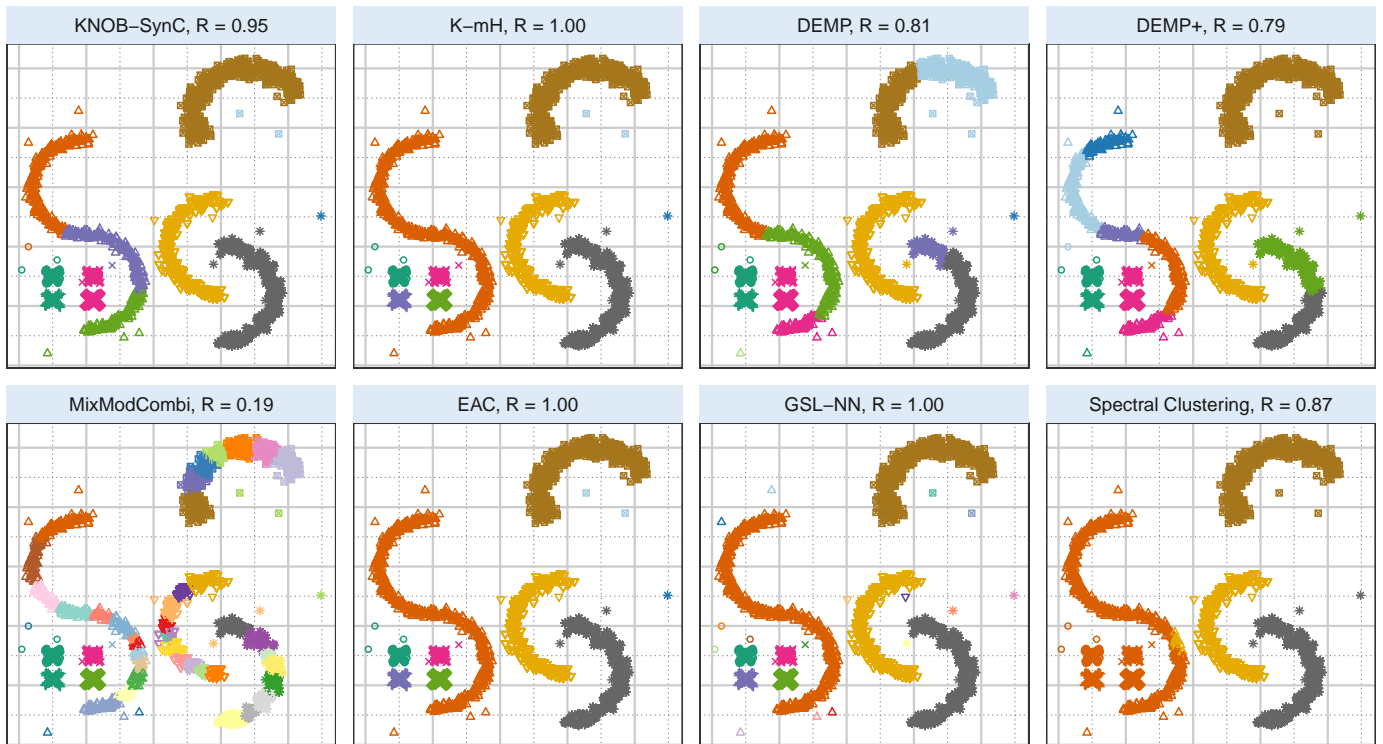


Fig. 16: Classifications obtained using the 8 algorithms on the SCX-Bananas dataset.

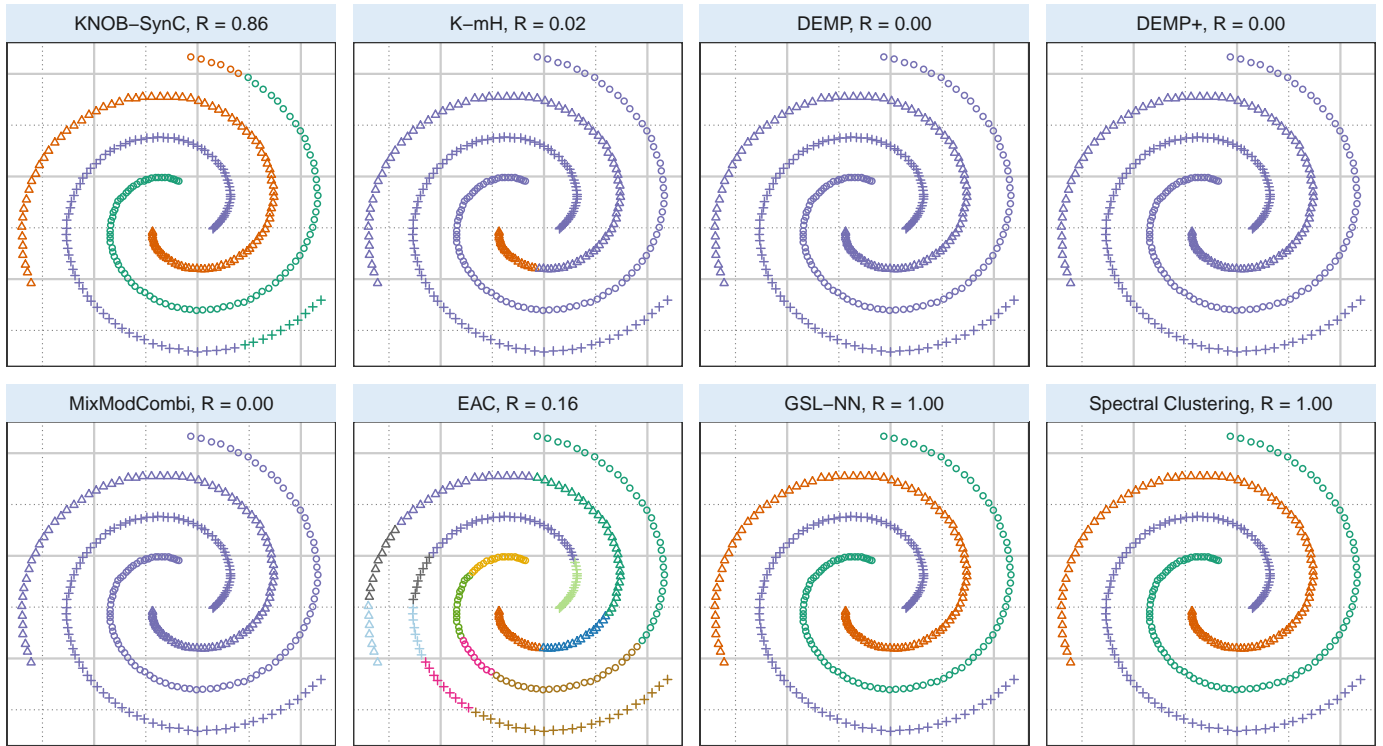


Fig. 17: Groupings of the Spiral dataset, obtained as per the 8 clustering algorithms.

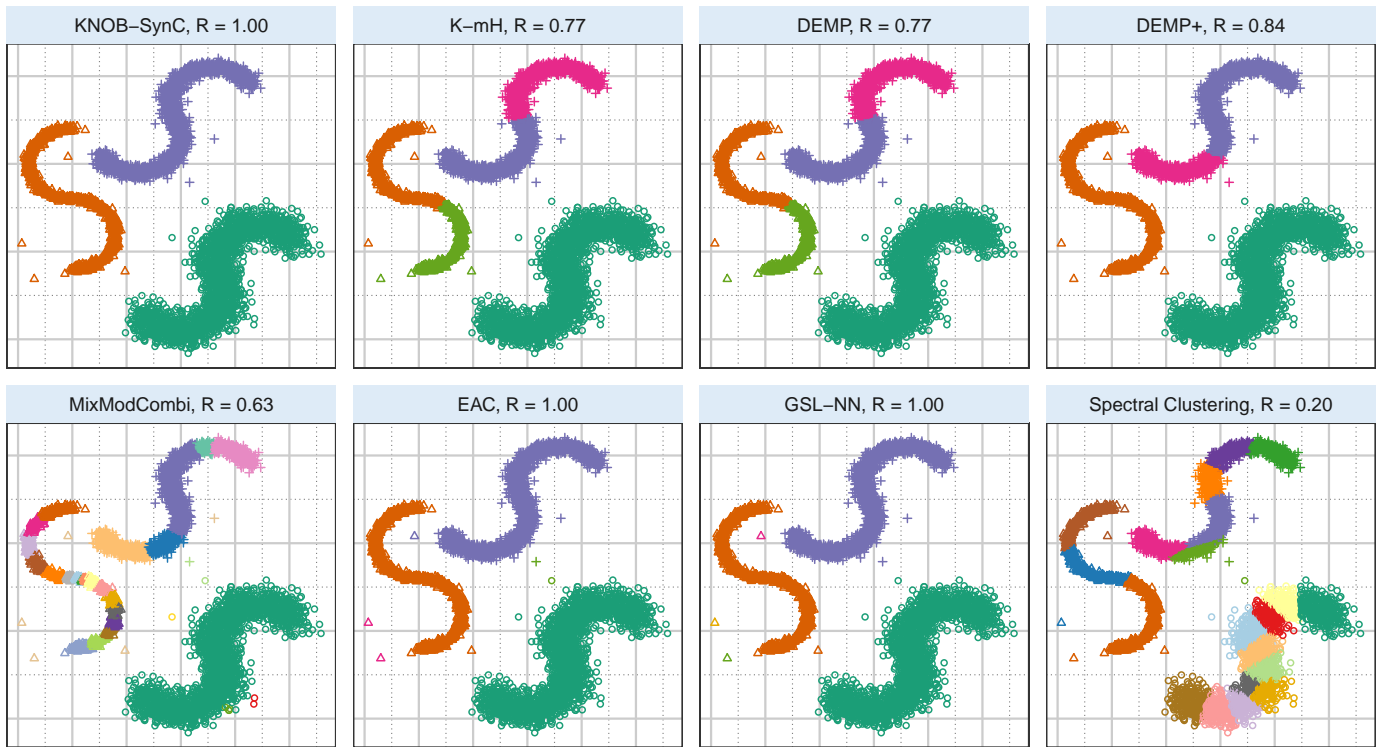


Fig. 18: Classifications of the SSS dataset, as obtained by the 8 clustering algorithms.

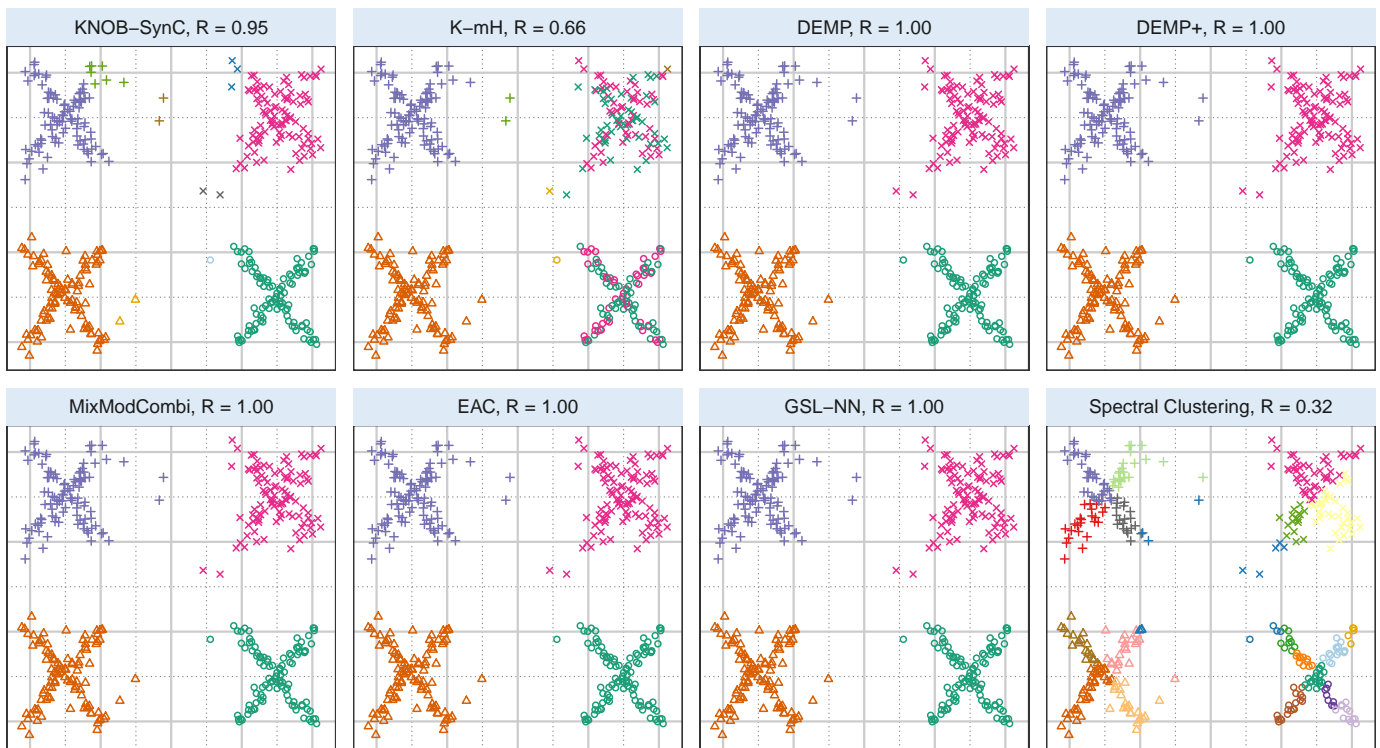


Fig. 19: Partitionings of the XXXX dataset, as obtained by 8 clustering algorithms.

- [2] D. B. Ramey, "Nonparametric clustering techniques," in *Encyclopedia of Statistical Science*. New York: Wiley, 1985, vol. 6, pp. 318–319.
- [3] G. J. McLachlan and K. E. Basford, *Mixture Models: Inference and Applications to Clustering*. New York: Marcel Dekker, 1988.
- [4] L. Kaufman and P. J. Rousseeuw, *Finding Groups in Data*. New York: John Wiley & Sons, 1990.
- [5] B. S. Everitt, S. Landau, and M. Leesem, *Cluster Analysis (4th ed.)*. New York: Hodder Arnold, 2001.
- [6] C. Fraley and A. E. Raftery, "Model-based clustering, discriminant analysis, and density estimation," *Journal of the American Statistical Association*, vol. 97, pp. 611–631, 2002.
- [7] R. J. Tibshirani and G. Walther, "Cluster validation by prediction strength," *Journal of Computational and Graphical Statistics*, vol. 14, no. 3, pp. 511–528, 2005.
- [8] J. R. Kettenring, "The practice of cluster analysis," *Journal of classification*, vol. 23, pp. 3–30, 2006.
- [9] R. Xu and D. C. Wunsch, *Clustering*. NJ, Hoboken: John Wiley & Sons, 2009.
- [10] C. D. Michener and R. R. Sokal, "A quantitative approach to a problem in classification," *Evolution*, vol. 11, pp. 130–162, 1957.
- [11] A. Hinneburg and D. Keim, "Cluster discovery methods for large databases: from the past to the future," in *Proceedings of the ACM SIGMOD International Conference on the Management of Data*, 1999.
- [12] R. Maitra, "Clustering massive datasets with applications to software metrics and tomography," *Technometrics*, vol. 43, no. 3, pp. 336–346, 2001.
- [13] S. Johnson, "Hierarchical clustering schemes," *Psychometrika*, vol. 32:3, pp. 241–254, 1967.
- [14] A. Jain and R. Dubes, *Algorithms for clustering data*. Englewood Cliffs, NJ: Prentice Hall, 1988.
- [15] E. Forgy, "Cluster analysis of multivariate data: efficiency vs. interpretability of classifications," *Biometrics*, vol. 21, pp. 768–780, 1965.
- [16] J. MacQueen, "Some methods for classification and analysis of multivariate observations," *Proceedings of the Fifth Berkeley Symposium*, vol. 1, pp. 281–297, 1967.
- [17] D. Titterton, A. Smith, and U. Makov, *Statistical Analysis of Finite Mixture Distributions*. Chichester, U.K.: John Wiley & Sons, 1985.
- [18] G. McLachlan and D. Peel, *Finite Mixture Models*. New York: John Wiley and Sons, Inc., 2000.
- [19] V. Melnykov and R. Maitra, "Finite mixture models and model-based clustering," *Statistics Surveys*, vol. 4, pp. 80–116, 2010.
- [20] J. A. Hartigan and M. A. Wong, "A k -means clustering algorithm," *Applied Statistics*, vol. 28, pp. 100–108, 1979.
- [21] S. Lloyd, "Least squares quantization in pcm," *Information Theory, IEEE Transactions on*, vol. 28, no. 2, pp. 129–137, 1982.
- [22] I. Dhillon, Y. Guan, and B. Kulis, "A unified view of kernel k -means, spectral clustering and graph cuts," University of Texas at Austin, Tech. Rep. TR-04-25, 2004.
- [23] A. L. Fred and A. K. Jain, "Combining multiple clusterings using evidence accumulation," *IEEE transactions on pattern analysis and machine intelligence*, vol. 27, no. 6, pp. 835–850, 2005.
- [24] U. von Luxburg, "A tutorial on spectral clustering," *Statistics and Computing*, vol. 17, no. 4, pp. 395–416, December 2007.
- [25] J.-P. Baudry, A. E. Raftery, G. Celeux, K. Lo, and R. Gottardo, "Combining mixture components for clustering," *Journal of Computational and Graphical Statistics*, vol. 19, no. 2, pp. 332 – 353, 2010.

- [26] C. Hennig, "Methods for merging Gaussian mixture components," *Advances in Data Analysis and Classification*, 2010.
- [27] V. Melnykov, "Merging mixture components for clustering through pairwise overlap," *Journal of Computational and Graphical Statistics*, vol. 25, no. 1, pp. 66–90, 2016.
- [28] A. D. Peterson, A. P. Ghosh, and R. Maitra, "Merging k -means with hierarchical clustering for identifying general-shaped groups," *Stat*, vol. 7, no. 1, p. e172, 2018.
- [29] W. Stuetzle and R. Nugent, "A generalized single linkage method for estimating the cluster tree of a density," *Journal of Computational and Graphical Statistics*, 2010.
- [30] R Development Core Team, *R: A Language and Environment for Statistical Computing*, R Foundation for Statistical Computing, Vienna, Austria, 2018, ISBN 3-900051-07-0. [Online]. Available: <http://www.R-project.org>
- [31] J.-P. Baudry and G. Celeux, *RmixmodCombi: Combining Mixture Components for Clustering*, 2014, r package version 1.0. [Online]. Available: <https://CRAN.R-project.org/package=RmixmodCombi>
- [32] R. Maitra and V. Melnykov, "Simulating data to study performance of finite mixture modeling and clustering algorithms," *Journal of Computational and Graphical Statistics*, vol. 19, no. 2, pp. 354–376, 2010.
- [33] C. Fraley and A. E. Raftery, "How many clusters? which cluster method? answers via model-based cluster analysis," *Computer Journal*, vol. 41, pp. 578–588, 1998.
- [34] D. Peel and G. McLachlan, "Robust mixture modeling using the t distribution," *Statistics and Computing*, vol. 10, p. 339:348, 2000.
- [35] R. Maitra, "A re-defined and generalized percent-overlap-of-activation measure for studies of fMRI reproducibility and its use in identifying outlier activation maps," *Neuroimage*, vol. 50, no. 1, pp. 124–135, 2010.
- [36] V. Melnykov and R. Maitra, "CARP: Software for fishing out good clustering algorithms," *Journal of Machine Learning Research*, vol. 12, pp. 69 – 73, 2011.
- [37] V. Melnykov, W.-C. Chen, and R. Maitra, "MixSim: An R package for simulating data to study performance of clustering algorithms," *Journal of Statistical Software*, vol. 51, no. 12, pp. 1–25, 2012. [Online]. Available: <http://www.jstatsoft.org/v51/i12/>
- [38] C. A. Sugar and G. M. James, "Finding the number of clusters in a dataset," *Journal of the American Statistical Association*, vol. 98, no. 463, 2003.
- [39] B. W. Silverman, *Density Estimation for Statistics and Data Analysis*. London: Chapman & Hall/CRC, 1986.
- [40] M. Rosenblatt, "Remarks on some nonparametric estimates of a density function," *The Annals of Mathematical Statistics*, vol. 27, no. 3, p. 832, 1956.
- [41] E. Parzen, "On estimation of a probability density function and mode," *The Annals of Mathematical Statistics*, vol. 33, no. 3, p. 1065, 1962.
- [42] M. P. Wand and M. C. Jones, *Kernel Smoothing*. London: Chapman & Hall/CRC, 1995.
- [43] V. A. Epanechnikov, "Non-parametric estimation of a multivariate probability density," *Theory of Probability and its Applications*, vol. 14, p. 153:158, 1969.
- [44] A. Azzalini, "A note on the estimation of a distribution function and quantiles by a kernel method," *Biometrika*, vol. 68, no. 1, pp. 326–328, 1981.
- [45] R.-D. Reiss, "Nonparametric estimation of smooth distribution functions," *Scandinavian Journal of Statistics*, pp. 116–119, 1981.
- [46] T. Bouezmarni and O. Scaillet, "Consistency of asymmetric kernel density estimators and smoothed histograms with application to income data," *Econometric Theory*, vol. 21, no. 02, pp. 390–412, 2005.
- [47] S. X. Chen, "Probability density function estimation using gamma kernels," *Annals of the Institute of Statistical Mathematics*, vol. 52, no. 3, pp. 471–480, 2000.
- [48] Y. Jeon and J. H. T. Kim, "A gamma kernel density estimation for insurance loss data," *Insurance: Mathematics and Economics*, vol. 53, pp. 569–579, 2013.
- [49] O. Scaillet, "Density estimation using inverse and reciprocal inverse gaussian kernels," *Nonparametric Statistics*, vol. 16, no. 1-2, pp. 217–226, 2004.
- [50] R. Maitra, V. Melnykov, and S. Lahiri, "Bootstrapping for significance of compact clusters in multi-dimensional datasets," *Journal of the American Statistical Association*, vol. 107, no. 497, pp. 378–392, 2012.
- [51] W. J. Krzanowski and Y. Lai, "A criterion for determining the number of groups in a data set using sum-of-squares clustering," *Biometrics*, pp. 23–34, 1988.
- [52] Z. Huang, "Clustering large data sets with mixed numeric and categorical values," in *Proceedings of the First Pacific Asia Knowledge Discovery and Data Mining Conference*. Singapore: World Scientific, 1997, p. 2134.
- [53] —, "Extensions to the k -means algorithm for clustering large data sets with categorical values," *Data Mining and Knowledge Discovery*, vol. 2, p. 283:304, 1998.
- [54] B. D. Ripley, *Stochastic Simulation*. Wiley, 1987.
- [55] R. B. Nelsen, *An Introduction to Copulas*, 2nd ed. New York: Springer, 2006.
- [56] A. Gionis, H. Mannila, and P. Tsaparas, "Clustering aggregation," *ACM Transactions on Knowledge Discovery from Data (TKDD)*, vol. 1, no. 1, p. 4, 2007.
- [57] L. Hubert and P. Arabie, "Comparing partitions," *Journal of Classification*, vol. 2, pp. 193–218, 1985.
- [58] R. Maitra, "Initializing partition-optimization algorithms," *IEEE/ACM Transactions on Computational Biology and Bioinformatics*, vol. 6, pp. 144–157, 2009. [Online]. Available: <http://doi.ieeecomputersociety.org/10.1109/TCBB.2007.70244>
- [59] C. T. Zahn, "Graph-theoretical methods for detecting and describing gestalt clusters," *IEEE Transactions on computers*, vol. 100, no. 1, pp. 68–86, 1971.
- [60] A. K. Jain and M. H. C. Law, "Data clustering: A users dilemma," in *Pattern Recognition and Machine Intelligence. PReMI 2005*, ser. Lecture Notes in Computer Science, S. K. Pal, B. S., and B. S., Eds., vol. 3776. Berlin, Heidelberg: Springer, 2005, pp. 1–10.
- [61] C. J. Veenman, M. J. T. Reinders, and E. Backer, "A maximum variance cluster algorithm," *IEEE Transactions on Pattern Analysis and Machine Intelligence*, vol. 24, no. 9, pp. 1273–1280, 2002.

- [62] D. J. Newman, S. Hettich, C. L. Blake, and C. J. Merz, "UCI repository of machine learning databases," 1998. [Online]. Available: [http://www.ics.uci.edu/\\$\sim\\$sim\\$mllearn/MLRepository.html](http://www.ics.uci.edu/\simsim$mllearn/MLRepository.html)
- [63] K. Nakai and M. Kinehasa, "Expert sytem for predicting protein localization sites in gram-negative bacteria," *PROTEINS: Structure, Function, and Genetics*, vol. 11, pp. 95–110, 1991.
- [64] P. Horton and K. Nakai, "A probabilistic classification system for predicting the cellular localization sites of proteins," *Intelligent Systems in Molecular Biology*, pp. 109–115, 1985.
- [65] R. Maitra, "A statistical perspective to data mining," *Journal of the Indian Society of Probability and Statistics*, vol. 6, pp. 28–77, 2002.
- [66] M. Forina, R. Leardi, and S. Lanteri, "PARVUS - an extendible package for data exploration, classification and correlation," Via Brigata Salerno, 16147 Genoa, Italy, 1988.
- [67] D. C. S. Aeberhard and O. de Vel, "Comparison of classifiers in high dimensional settings," Department of Computer Science and Department of Mathematics and Statistics, James Cook University of North Queensland, Tech. Rep. 92-02, 1992.
- [68] M. Forina and E. Tiscornia, "Pattern recognition methods in the prediction of italian olive oil origin by their fatty acid content," *Annali di Chimica*, vol. 72, pp. 143–155, 1982.
- [69] M. Forina, C. Armanino, S. Lanteri, and E. Tiscornia, "Classification of olive oils from their fatty acid composition," in *Food Research and Data Analysis*. London: Applied Science Publishers, 1983, pp. 189–214.
- [70] K. Nakai, "UCI machine learning repository," 1996. [Online]. Available: <http://archive.ics.uci.edu/ml>
- [71] E.-J. Yeoh, M. E. Ross, S. A. Shurtleff, W. Williams, D. Patel, R. Mahfouz, F. G. Behm, S. C. Raimondi, M. V. Relling, A. Patel, C. Cheng, D. Campana, D. Wilkins, X. Zhou, J. Li, H. Liu, C.-H. Pui, W. E. Evans, C. Naeve, L. Wong, and J. R. Downing, "Classification, subtype discovery, and prediction of outcome in pediatric acute lymphoblastic leukemia by gene expression profiling," *Cancer Cell*, vol. 1, no. 2, pp. 133 – 143, 2002. [Online]. Available: <http://www.sciencedirect.com/science/article/pii/S1535610802000326>
- [72] F. Alimoglu, "Combining multiple classifiers for pen-based handwritten digit recognition," Master's thesis, Institute of Graduate Studies in Science and Engineering, Bogazici University, 1996.
- [73] F. Alimoglu and E. Alpaydin, "Methods of combining multiple classifiers based on different representations for pen-based handwriting recognition," in *Proceedings of the Fifth Turkish Artificial Intelligence and Artificial Neural Networks Symposium (TAINN 96)*, Istanbul, Turkey, 1996.
- [74] T. Chattopadhyay, R. Misra, A. K. Chattopadhyay, and M. Naskar, "Statistical evidence for three classes of gamma-ray bursts," *Astrophysical Journal*, vol. 667, no. 2, p. 1017, 2007. [Online]. Available: <http://stacks.iop.org/0004-637X/667/i=2/a=1017>
- [75] T. Piran, "The physics of gamma-ray bursts," *Rev. Mod. Phys.*, vol. 76, pp. 1143–1210, Jan 2005. [Online]. Available: <http://link.aps.org/doi/10.1103/RevModPhys.76.1143>
- [76] E. P. Mazets, S. V. Golenetskii, V. N. Ilinskii, V. N. Panov, R. L. Aptekar, I. A. Gurian, M. P. Proskura, I. A. Sokolov, Z. I. Sokolova, and T. V. Kharitonova, "Catalog of cosmic gamma-ray bursts from the KONUS experiment data. I," *Astrophysics and Space Science*, vol. 80, pp. 3–83, Nov. 1981.
- [77] J. P. Norris, T. L. Cline, U. D. Desai, and B. J. Teegarden, "Frequency of fast, narrow gamma-ray bursts," *Nature*, vol. 308, p. 434, Mar. 1984.
- [78] J.-P. Dezalay, C. Barat, R. Talon, R. Syunyaev, O. Terekhov, and A. Kuznetsov, "Short cosmic events - A subset of classical GRBs?" in *American Institute of Physics Conference Series*, ser. American Institute of Physics Conference Series, W. S. Paciesas and G. J. Fishman, Eds., vol. 265, 1992, pp. 304–309.
- [79] S. Mukherjee, E. D. Feigelson, G. Jogesh Babu, F. Murtagh, C. Fraley, and A. Raftery, "Three types of gamma-ray bursts," *Astrophysical Journal*, vol. 508, pp. 314–327, Nov. 1998.
- [80] S. Chattopadhyay and R. Maitra, "Gaussian-mixture-model-based cluster analysis finds five kinds of gamma-ray bursts in the batse catalogue," *Monthly Notices of the Royal Astronomical Society*, vol. 469, no. 3, pp. 3374–3389, 2017. [Online]. Available: [+http://dx.doi.org/10.1093/mnras/stx1024](http://dx.doi.org/10.1093/mnras/stx1024)
- [81] S. Chattopadhyay and R. Maitra, "Multivariate *t*-Mixtures-Model-based Cluster Analysis of BATSE Catalog Establishes Importance of All Observed Parameters, Confirms Five Distinct Ellipsoidal Sub-populations of Gamma Ray Bursts," *ArXiv e-prints*, May 2018.
- [82] A. E. Raftery and N. Dean, "Variable selection for model-based clustering," *Journal of the American Statistical Association*, vol. 101, pp. 168–178, 2006.
- [83] G. Schwarz, "Estimating the dimensions of a model," *Annals of Statistics*, vol. 6, pp. 461–464, 1978.
- [84] P. A. Bandettini, A. Jesmanowicz, E. C. Wong, and J. S. Hyde, "Processing strategies for time-course data sets in functional mri of the human brain," *Magnetic Resonance in Medicine*, vol. 30, pp. 161–173, 1993.
- [85] J. W. Belliveau, D. N. Kennedy, R. C. McKinstry, B. R. Buchbinder, R. M. Weisskoff, M. S. Cohen, J. M. Vevea, T. J. Brady, and B. R. Rosen, "Functional mapping of the human visual cortex by magnetic resonance imaging," *Science*, vol. 254, pp. 716–719, 1991.
- [86] K. K. Kwong, J. W. Belliveau, D. A. Chesler, I. E. Goldberg, R. M. Weisskoff, B. P. Poncelet, D. N. Kennedy, B. E. Hoppel, M. S. Cohen, R. Turner, H.-M. Cheng, T. J. Brady, and B. R. Rosen, "Dynamic magnetic resonance imaging of human brain activity during primary sensory stimulation," *Proceedings of the National Academy of Sciences of the United States of America*, vol. 89, pp. 5675–5679, 1992.
- [87] S. Ogawa, T. M. Lee, A. S. Nayak, and P. Glynn, "Oxygenation-sensitive contrast in magnetic resonance image of rodent brain at high magnetic fields," *Magnetic Resonance in Medicine*, vol. 14, pp. 68–78, 1990.
- [88] K. J. Friston, P. Jezzard, and R. Turner, "Analysis of functional mri time-series," *Human Brain Mapping*, vol. 1, pp. 153–171, 1994.
- [89] G. H. Glover, "Deconvolution of impulse response in event-related bold fmri," *Neuroimage*, vol. 9, pp. 416–429, 1999.
- [90] N. A. Lazar, *The Statistical Analysis of Functional MRI Data*. Springer, 2008.
- [91] K. J. Friston, A. P. Holmes, K. J. Worsley, J.-B. Poline, C. D. Frith, and R. S. J. Frackowiak, "Statistical parametric maps in functional imaging: A general linear approach," *Human Brain Mapping*, vol. 2, pp. 189–210, 1995.

- [92] S. D. Forman, J. D. Cohen, M. Fitzgerald, W. F. Eddy, M. A. Mintun, and D. C. Noll, "Improved assessment of significant activation in functional magnetic resonance imaging (fmri): Use of a cluster-size threshold," *Magnetic Resonance in Medicine*, vol. 33, pp. 636–647, 1995.
- [93] C. R. Genovese, N. A. Lazar, and T. E. Nichols, "Thresholding of statistical maps in functional neuroimaging using the false discovery rate:," *Neuroimage*, vol. 15, pp. 870–878, 2002.
- [94] B. Thirion, G. Varoquaux, E. Dohmatob, and J.-B. Poline, "Which fmri clustering gives good brain parcellations?" *Frontiers in Neuroscience*, vol. 8, p. 167, 2014. [Online]. Available: <https://www.frontiersin.org/article/10.3389/fnins.2014.00167>
- [95] A. R. Nath and M. S. Beauchamp, "Dynamic changes in superior temporal sulcus connectivity during perception of noisy audiovisual speech," *The Journal of Neuroscience*, vol. 31, no. 5, p. 1704 1714, 2011.
- [96] R. W. Cox, "Afni: software for analysis and visualization of functional magnetic resonance neuroimages," *Computers and Biomedical research*, vol. 29, no. 3, pp. 162–173, 1996.